University of Zurich[UZH]

Terrestrial radar signal improvement by correction for atmospheric disturbances

GEO 511 Master's Thesis

Author
Anja Gloor
15-705-858

Supervised by
Dr. Martin Lüthi
Dr. Andrea Kneib-Walter
Dr. Daniel Henke

Faculty representative
Prof. Dr. Alexander Damm

31.01.2023
Department of Geography, University of Zurich

Contents

List of Figures

List of Tables

Acknowledgements

I would like to express my deep gratitude to Dr. Martin Lüthi, Dr. Andrea Kneib-Walter and Dr. Daniel Henke, my research supervisors, for their patient guidance, enthusiastic encouragement and useful critiques of this research work. Additionally, I would like to thank Dr. Martin Lüthi and Dr. Andrea Kneib-Walter for providing code which made working with the GPRI data possible.

I greatly thank Dr. Kathrin Naegeli, Laura Niggli, Kaspar Spring, Luzian Scharfenberger and Emanuel Büchler for their valuable feedback on my text. Finally, I would like to thank all my friends for their support and encouragement during this master thesis.

Abstract

Glaciers have a major impact on the world's climate and are therefore, along with other factors, the focus of research on climate change. There are many options to study glaciers and their condition. One of them is the speed of ice flow. In this paper, the ice flow velocity of the Gorner Glacier, which is located in the Swiss Alps, is studied. The main aim of this thesis is investigating the potential of terrestrial radar interferometry (TRI) to calculate the ice flow of a alpine glacier. A big challenge with radio detection and ranging (radar) is diffraction, which is the change in the optical properties of the atmosphere. Thus, it is visible on the GAMMA Portable Radar Interferometer (GPRI) measurements but is not the information one is interested in. This cause temporary phase shifts that can attain several phase cycles which significantly distorts the results.

There are several approaches to correct the atmospheric disturbances on radar images. In this master thesis, two of them are investigated. The first one was developed by Dr. Martin Lüthi from the Glaciology and Geomorphodynamics group at University of Zurich. His approach is to model the ice flow by the assumption that the ice moves regularly and particularly in the same direction. Thus, the phase shift of an ice pixel should show a clear trend. The irregular movements of the phase shift is noise and among others the mentioned atmospheric disturbance. To correct the atmospheric disturbance, it is assumed that the disturbance is similar on one azimuth line, so the extracted noise is grouped over them and a general noise pattern is subtracted from the original radar signal. The second algorithm corrects the atmospheric disturbance by an adaptive filtering of multi-looking images, which was developed by Goldstein and C. L. Werner (1998) and is an often used approach.

The effectiveness of correcting for atmospheric disturbance using the extracted noise was not fully confirmed. When comparing the results with correction by an adaptive filter it was revealed relatively similar results. The calculations using GPRI data were verified using control points based on independent photogrammetry data from uncrewed aerial vehicles (UAV). The modeling via GPRI data shows a significant underestimation of the velocity of the ice flow compared to the UAV control points. It can be assumed that this underestimation could be significantly improved if the location of the GPRI were chosen more favourably or by implementing a correction factor of the angle. Furthermore, it became clear that both algorithms, which are based on the GPRI data, show only small changes in the calculated velocities before and after the correction. The atmospheric disturbance is very complex and requires more sophisticated approaches, whereby a combination between different approaches and an optimal selection of data is to be preferred.

Keywords

climate change, glacier, glaciology, ice flow velocity, radar, remote sensing, terrestrial radar interferometry

1 Introduction

Glaciers have always played an important role in the history of mankind. In many mythologies around the world, glaciers are inhabited of demons, goblins, dragons and giants, while many are about the destructive force of glacier advance. The history of glacier research is based on the advent of classical physics and a romantic enthusiasm for nature, which can be traced back to the eighteenth and nineteenth century (Clarke, 1987).

"The air immediately above me seemed filled with rainbow-dust, for the ice-needles glittered with a thousand hues under the decomposition of light upon them, while the dark storm in the valley below offered a strange contrast to the brilliancy of the upper region in which I stood". - Louis Agassiz

After some 200 years of glacier research, and thanks to a large community of multidisciplinary scientists around the world, a vast body of knowledge exists about glaciers and the processes that affect and are affected by them. In recent decades, research has focused largely on the effects of climate change on glaciers and, in turn, its impact on the environment.

This section will first elaborate on the importance of research in glaciology, focusing on ice flow of an alpine glacier. Methods will be introduced how to determine the flow rate of a glacier, while the focus lays on remote sensing techniques and in particular on radio detection and ranging (radar). In the second section, two different algorithms are introduced which are intended to correct atmospheric disturbances on radar measurements in order to calculate the phase shift caused by the ice movement. This includes the two mentioned algorithms that are processed on data from a GAMMA Portable Radar Interferometer (GPRI) as well as possible improvements. Additionally, UAV data are used for validation. The results of the analysis are presented in section 3, and will be discussed in section 4. This master thesis concludes with a summary and reflection of the done analysis as well as an outlook on further work in the conclusion (section 5).

1.1 Glaciers and why it's important to understand them

Directly or indirectly, all people are affected by glaciers. Fresh water from the cryosphere is released seasonally into rivers through ablation. Hence, glaciers provide life-sustaining water for the human population, as well as wildlife and plants. Moreover, dust particles containing bacteria, viruses, fungi, small protists, pollen grains, seeds as well as plant and insect fragments, originating from different locations around the globe, are carried by aeolian

systems and deposited on the surface by rain and snowfall. Therefore, glacier melt delivers this vital nutrients into lakes, rivers, and oceans, which can drive blooms of phytoplankton, which are fundamental for aquatic and marine food chains (Pörtner et al., 2019; Miteva, 2008). But the microorganisms contained in the ice not only serve as nutrition in hydrologic systems but also provide information about the origin, evolution and limits of life on Earth and possibly on other planets, as it preserves past climate changes chronologically for hundreds of thousands of years (Miteva, 2008). Especially, for people living in close vicinity of the cryosphere, these systems provide essential livelihoods, food security, well-being and cultural identity. With steadily increasing temperatures, due to climate change, glacier melt has increased significantly, which is causing a rapid release of fresh water to the earth's water cycle. These developments have consequences: If all the water currently stored as ice in the polar ice caps and glaciers is released, global sea level will rise about 0.5 m. And this approximation excludes the ice sheets of Antarctica and Greenland, which currently hold 77% of the water in ice. About 200 million people live in places which will be below the high-tide line of rising sea levels by the end of the century (Voytenko, 2015; Pörtner et al., 2019; Hugonnet et al., 2021; Zemp et al., 2019). Glacier melt is essential for the freshwater supply of 1.9 billion people who live in alpine regions (Immerzeel et al., 2019). However, only a certain amount of this seasonal melt water can be used directly or stored for later. Anything beyond this capacity seeps into the ground and is no longer available to these regions (Voytenko, 2015; Huss and Hock, 2018). Furthermore, glacier- and permafrost-related hazards, such as outbursts of glacier lakes, ice break-offs and subsequent ice avalanches, glacier length variations, destabilisation of frozen or unfrozen debris slopes and destabilisation of rock walls, have increasingly observed in recent decades due to glacier retreat. Events arising from these hazards can kill many people and cause huge property damage (L. Fischer et al., 2006; Kääb, Reynolds, and Haeberli, 2005).

The before mentioned impending catastrophic impacts of climate change on glaciers and the associated hazards and risks (Vuille et al., 2008; Vincent, 2002; Kaser et al., 2004; Sagredo and Lowell, 2012), as well as models for future scenarios of climate change (Akhtar, Ahmad, and Booij, 2008; Bliss, Hock, and Radić, 2014) are a widespread topic in contemporary glaciology research papers. For several reasons, it is essential to understand how glaciers will change in the coming decades and what processes will be triggered by these changes. For example, it may prove necessary to develop early warning systems to ensure the safety of people in larger areas around glaciers. Or when entire glaciers have disappeared and no longer provide the necessary supply of fresh water to that region, new solutions on how to build up, store and distribute water must be developed such as man-made ice towers (Palmer, 2022) or the development of water filters for salt and waste water (Islam et al., 2022).

It is well known that ice flows downhill by internal deformation of the ice, sliding and bed deformation at the base. The rate at which this occurs is mainly controlled by surface slope, ice thickness, the effective ice viscosity, and basal thermal and physical conditions (Houghton et al., 2001). Ever since the last glacier advances ended in the 1980's, ice flow velocities have significantly and continuously decreased (C. Werner et al., 2009; Strozzi, C. Werner, et al., 2012; X. Li et al., 2016; Wang et al., 2021). When considering the simultaneous glacier retreat, it becomes reasonable to conclude that ice flow velocity is a good indicator of the condition of a glacier.

1.2 State of knowledge of radar remote sensing

Aim of this thesis is to investigate the ice flow velocity of the Gorner Glacier in the Swiss alps, in order to find robust methods to make large-scale and spatially high-resolution measurements of the ice flow velocity. The next section introduces the current state of the art methods to measure ice flow velocity with the use of radar. It will be followed up with at short introduction of the technology which was ultimately chosen to carry out the measurements.

1.2.1 Radar remote sensing for ice flow velocity measurements

Broadly speaking, there are two methods to obtain measurement data for ice flow velocity calculations: by making in-situ measurements or the use of remote sensing techniques. The former methods, such as point observations (Ai et al., 2019; Fu, Guo, and Chen, 2021), offer the advantage of high sub-millimeter accuracy but come with the disadvantages of low spatial resolution and the necessity of being on site. However, this is not feasible in many Alpine regions due to poor approachability and unfavourable weather conditions (Bhardwaj and Sam, 2022). In such scenarios, remote sensing approaches are more commonly implemented, as these prove to be more convenient than field studies. But these methods also come with downsides. While, for example, aerial photogrammetry and airborne laser scanning, can be used to survey spatially extensive areas and provide very large spatial coverage. However, the resulting change detection is often much less accurate than the results of point surveys due to lower spatial resolution. Another remote sensing technique, offered by satellite synthetic aperture radar (SAR) can support high spatial coverage, high spatial resolution and high precision (millimeter-scale) for assessment of surface changes when differential interferometry is used (Caduff, Schlunegger, et al., 2015; Fischer and Andrea, 2013). Long period analysis has been made for several years to asses changes over time (C. Werner et al., 2009; Strozzi, C. Werner, et al., 2012). However, SAR still has the substantial limitation that the observation

period is restricted to the time the satellite passes and revisits the target on appropriate orbits. The revisit time of a satellite sensor is usually several days, which drastically limits the temporal resolution (Ferretti et al., 2007). These data are inadequate to track the rapid glacier changes, for example close to a calving front, where glaciers terminate in the ocean (C. Werner et al., 2009; Strozzi, C. Werner, et al., 2012). Furthermore, SAR is limited by the sensitivity to atmospheric artefacts, phase ambiguity and the determination of displacements along line-of-sight. Terrestrial Radar Interferometry (TRI) can overcome most of the mentioned limitations. Due to its minute-scale observation interval TRI is vital to observe rapid processes and has demonstrated its capability to research rapid glacier change, two-dimensional velocity change of glacier, grounding line variation, calving process and glacier strain (C. Werner et al., 2009; Strozzi, C. Werner, et al., 2012). Additionally, due to the possibility of very short revisit-time the temporal decorrelation can be reduced to a minimum by choosing a suitable measurement interval. Another difference to space or airborne systems, terrestrial radar interferometers offer the advantage that the antenna-position does not change between two acquisitions, which is called zero-baseline. So the determination of displacements along line-of-sight due to the movement of the sensor, as is the case with SAR, can be neglected. But there is still the challenge of atmospheric artefacts and noise. Especially during daytime, blobs of air with different refraction properties rapidly move through the area of interest and cause temporary phase shifts that can attain several phase cycles (Biondi, Clemente, and Orlando, 2019). The possibilities of correcting atmospheric disturbances on radar images will be discussed in more detail in the following section.

1.2.2 GPRI signal improvement

The advantages and disadvantages of radar have been known for a long time and therefore there is a wide range of methods to improve the quality of radar measurements. This section focuses exclusively on the correction of atmospheric disturbances. In the past, attempts were made to model the atmospheric artefacts by looking at air temperatures, pressures and water vapor contents in the corresponding region (Zebker, Rosen, and Hensley, 1997; Iannini and Monti Guarnieri, 2011).

Another frequently used approach is to normalise the data using a stable reference point. Allstadt et al. (2015), Voytenko et al. (2012) and Monserrat, Crosetto, and Luzi (2014) observed that the scale of the atmospheric noise features were typically much wider than the width of the glaciers, so in order to minimize this atmospheric noise in the individual interferograms, they interpolated apparent displacement values over static control surfaces for example exposed bedrocks.

Alternatively, the stacking of interferograms over a specific time interval offers the possi-

bility of averaging a set of independent interferograms, which results in a significant reduction of phase noise and turbulent atmospheric components (Strozzi, Wegmuller, et al., 2001; Kneib-Walter, Lüthi, Moreau, et al., 2021; Kneib-Walter, Lüthi, Funk, et al., 2022).

There are many other attempts (Luzi et al., 2004; Iglesias et al., 2014; Caduff, Kos, et al., 2014; Allstadt et al., 2015) to remove the atmospheric disturbances from radar images. However, it is striking that most cases are targeted to distinguish the disturbances from the actual mass movement on the ground and thus to be able to correct for them specifically. This approach is also followed by the algorithm developed by Dr. Martin Lüthi, which is explained in more detail in section 2.3 and examined deeply in this thesis.

1.3 Study area

The radar measurements were taken from Gorner Glacier which is located in the Valais Alps in southern Switzerland and ranges from 2200 m to 4634 m above sea level. The Gorner Glacier has a about 4 km long and relatively flat ice tongue that is partially debris covered and is deeply incised by melt water channels. The upper ablation area consists of a steeper part (southwest of the Monte Rosa Hut), which is the main focus of this study, characterized by the presence of numerous crevasses. The entire Gorner Glacier system covers an area of almost 50 km^2 and its central flow line is 12 km long. These facts make it to one of the largest European glaciers (Benoit et al., 2019; Sugiyama et al., 2010). Figure 1 shows the outline of the Gorner Glacier on a map of the zermatt region, with the extent and the various accumulation zones clearly visible.

The Gorner Glacier has been intensively studied since the 1950s because of its considerable size, its accessibility, and because a lake dammed by the glacier threatened the downstream Mattertal valley with glacial outbursts (Renaud, 1952; Klingele and Kahle, 1977; Bauder et al., 2008; Lüthi and Bauder, 2010; Lüthi, Bauder, and Funk, 2010; Ryser et al., 2013; Lüthi, 2014; Irarrazaval et al., 2021). The long history of glaciological investigations in this area has shown that the mass balance of the Gorner Glacier system was stable from the 1930s to the early 1980s and has decreased significantly since then (Huss, Hock, et al., 2012). This may be associated with the increase in its equilibrium line altitude (ELA) due to an increase in local annual average temperature.

1.4 Research context, goals and research questions

The aim of this thesis is to evaluate two different algorithms that allow for a correction of the atmospheric disturbances of the radar signal. Thus, the following questions should be answered in this thesis:

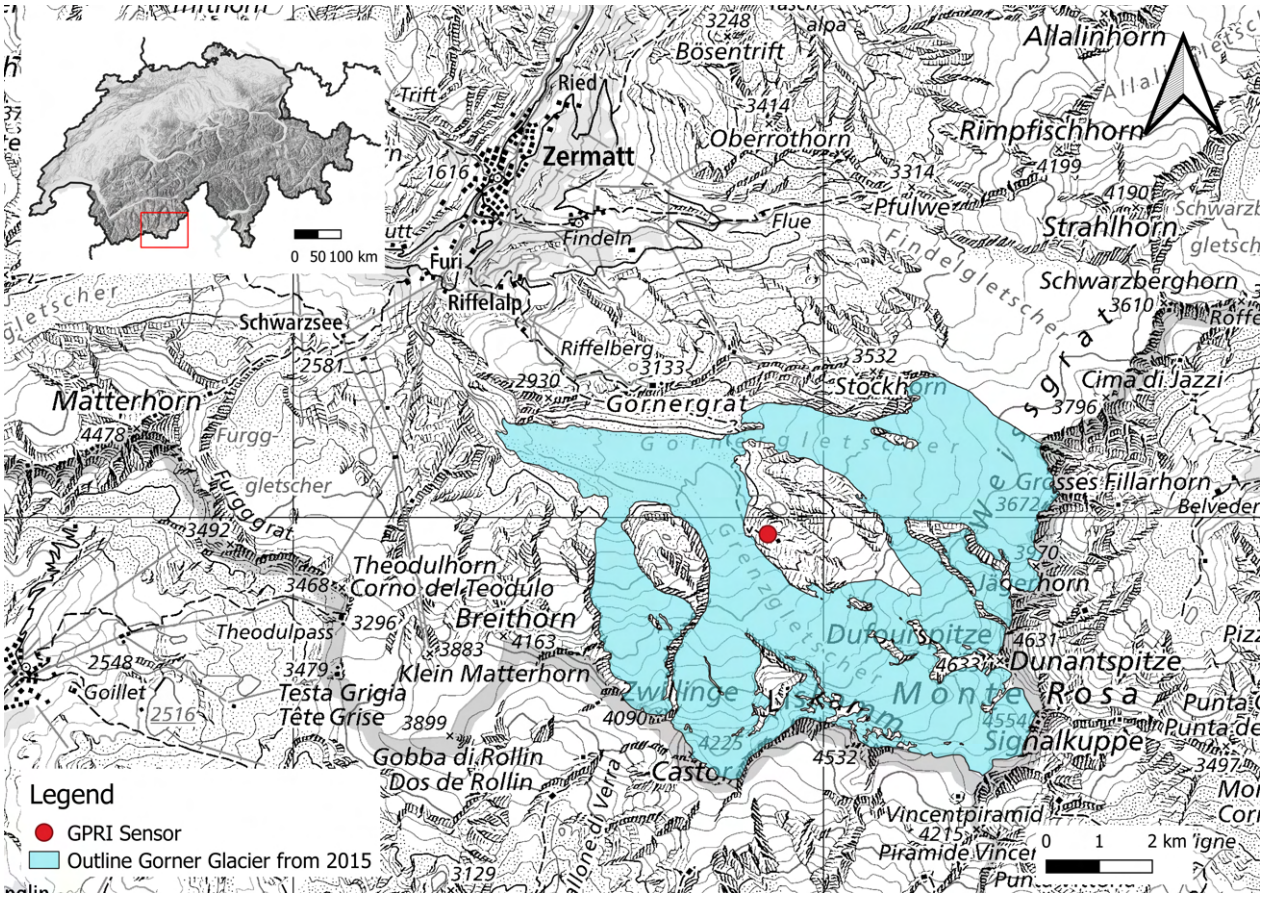

Figure 1: Overview of the study area. Glacier Outline from GLIMS Consortium (2005), relief, national map (grey) and national border of Switzerland from Bundesamt für Landestopografie swisstopo (2021).

RQ1 Can the atmospheric disturbance be corrected enough to calculate the glacier's flow rate plausibly?

RQ2 Can a significant difference be found between the two algorithms?

RQ3 If the second research question (RQ2) answered with yes, which of the two investigated algorithms is better suited for the correction of atmospheric disturbance?

2 Methodology

To answer the research questions, a quantitative analysis of two algorithms was performed using radar images of a GPRI. Subsequently, the results of the two algorithms were compared with UAV independent photogrammetry data to determine whether the algorithms provide plausible results. In the following subchapters, the basic principles of radar and GPRI and the investigated algorithms are explained, as well as the data that were worked with.

2.1 Introduction to radar remote sensing

The first applications of imaging radar remote sensing were used for military reconnaissance purposes in the late 1940s (Lillesand, Kiefer, and Chipman, 2015). The big advantages compared to photogrammetry were in particular the possibility to take pictures in almost any weather condition and at day and night times because of the active system approach (Lillesand, Kiefer, and Chipman, 2015).

Radar transmits a pulse of microwave beams in the direction of interest and measures the strength of the returned signal, which represents the backscattering capability and therefore it is related to the roughness and material properties of the terrain of the corresponding ground pixel, this information is called the amplitude. As well as the position in the microwave interval (2π) when the returned signal is detected by the receiver, thus it doesn't measure the total beam history. Rather, it measures only a fraction of a wavelength that remains after subtracting all full intervals, this information is known as phase. Figure 2 shows the relationship between phase, amplitude and the wavelength of a radar beam.

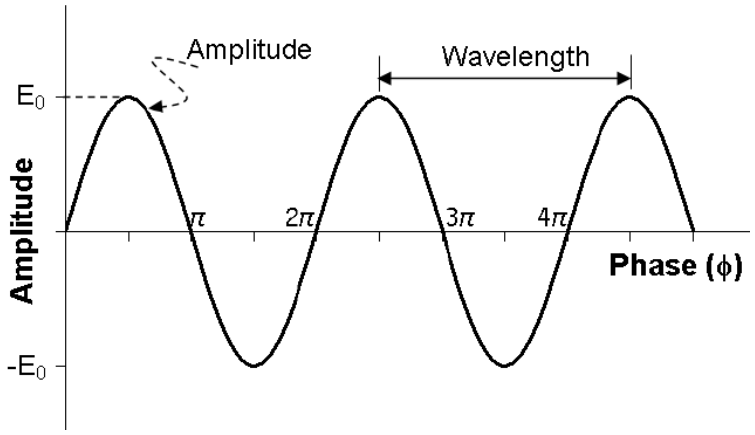

Figure 2: The relationship between phase, amplitude and the wavelength of a radar beam (Zhou, Chang, and S. Li, 2009).

The intensity of the returned signal is defined as squared amplitude. It is important to mention that backscattering and reflection are two different concepts. A calm water surface is very reflective but characterised by the least backscattering, therefore calm water surfaces correspond to dark pixels in radar images (Zhou, Chang, and S. Li, 2009). In addition, a radar can transmit a microwave beam horizontally or vertically polarized, and distinguish that polarization when receiving the returned signal. The polarization can provide information about the texture of the reflectors. The earlier returned signal is recorded first and for each scan, line observation in azimuth direction is recorded from near range to far range and observations from multiple azimuth lines construct one scanning image (C. Werner et al., 2009; Strozzi, C. Werner, et al., 2012).

The digitized signal from a ground pixel is conveniently represented as a complex value which contains a real (re) and a imaginary (im) component. This results in the following relationships. Where the amplitude (A), the intensity (I) and the phase (P) are given by:

$$A = \sqrt{(re^2 + im^2)} \Rightarrow I = (\sqrt{(re^2 + im^2)})^2 = re^2 + im^2 \tag{1}$$

$$P = \arctan\left(\frac{im}{re}\right) \tag{2}$$

The raw radar data are stored in a single-look complex (SLC) format. Single-look implies that the data have not been spatially averaged, while complex refers to the fact that every pixel in azimuth and range contains a complex value related to the amplitude and phase information of the measured signal.

In this thesis, we are particularly concerned with how the phase of a pixel changes over time. The phase of the resolution element is an average of many different scatterers within the pixel, and each resolution element has a random phase. If there is no motion and the atmosphere remains constant, then the phase does not change between acquisitions. Since the phase measurements are very precise, we can compare two of them acquired at different times to measure displacement of the target (pixel). Here we have to be aware that all phase differences fall within one cycle of a wave, and thus range over an interval of 2π, this is called wrapped radar signal. Wrapping poses a problem if motion exceeds one cycle of the wave, the measurement will appear as only a fraction of a cycle. Therefore, to resolve the phase ambiguities and to generate reasonable motion measurements, the phase is unwrapped (Zhou, Chang, and S. Li, 2009).

By evaluating the time between transmitting and receiving of the beam, the distance,

also named as range, can be determined. Assuming that energy propagates in air at about the speed of light c, the slant range ($\overline{SR}$) to an object is given by

$$\overline{SR} = \frac{ct}{2} \tag{3}$$

While

$\overline{SR}$ = the distance travelled by a radar beam (slant range). Thus, this distance needs to be divided by 2 so that the direct distance between transmitter and object is obtained

c = the speed of light (3×10^8 m/s) and

t = the time between pulse transmission and echo reception

(Lillesand, Kiefer, and Chipman, 2015).

2.2 GAMMA Portable Radar Interferometer

The GAMMA Portable radar Interferometer (GPRI) is a ground-based real-aperture radar system which has one transmitter antenna that emits waves in Ku-Band with 17.2 GHz and two receiver antennas which measure the reflected energy. Figure 3 shows a picture of the GPRI which was used to collect the GPRI data for this thesis. The signals from the two simultaneously working receiving antennas can be combined to generate an interferogram, since the antennas have a small distance between each other. The system can be installed rapidly and provides very high temporal and spatial resolution data due to the fixed location and the short distance to our target.

2.3 Correction of the atmospheric disturbance on the GPRI data

As already explained in previous sections, radar remote sensing has great advantages but also challenges. One of them is diffraction, which is the change in the optical properties, of the atmosphere and are visible on the GPRI measurements but is not the information one is interested in. Especially during daytime, blobs of air with different refraction properties rapidly move through the area of interest and cause temporary phase shifts that can attain several phase cycles. In this thesis two algorithm will be implemented to enhance the data quality of the GPRI by correcting the atmospheric disturbance due to radar reflection. The first algorithm, which will be explained in section 2.3.1, was developed by Dr. Martin Lüthi from the Institute of Glaciology and Geomorphodynamics at the University of Zurich. The second

Figure 3: GAMMA Portable Radar Interferometer installed above Gorner Glacier

algorithm in the following section 2.3.2 is a very simple but often implemented approach which uses multi looking and adaptive filtering to get rid of the atmospheric artefacts.

2.3.1 1st algorithm - the trend approach

The first algorithm calculates the noise which is then subtracted from the original data. It is assumed that the atmospheric disturbance is the same along one azimuth line and that the motion does not change direction during the measurement period and the velocity is approximately constant. Accordingly, a linear trend in the phase pattern is expected. The trend can be positive or negative depending whether the glacier is moving towards (positive trend) or away (negative trend) from the sensor.

For each azimuth line, the phase change is analyzed pixel by pixel over a meaningful selection of measurements. The criteria on which the selection was made are described in more detail in subsection 2.3.1.1. First the phase gets unwrapped. Now the assumption is evident that the movement of the glacier shows a trend over time. To get the noise, this

trend is removed from the phase change. This steps have to be repeated for all pixels of the azimuth line, which ends up with n, where n is the number of pixels per azimuth line, unwrapped and detrended phases. Since the atmospheric disturbance is assumed to have a similar pattern over an azimuth line, the phase with the greatest similarity is evaluated by clustering. This phase, which thus represents the modeled atmospheric disturbance, is now subtracted again from the original phase.

The effective trend can be quantified by a polynomial fit of a linear function. With the following formula the slope of the linear function found is converted into the ice flow velocity (v) in meter per day.

$$v = a \cdot \frac{\frac{w}{2}}{2\pi} \cdot 3600 \cdot 24 \tag{4}$$

Where a is the slope of the linear function and w the transmitted and received wavelenghth from the GPRI. We get v as the velocity in meter per day.

The basics of the code of the first algorithm und a lot of useful tools to work with GPRI data were provided by Dr. Martin Lüthi.

2.3.1.1 Selection of good and low-noise data

The best strategy to get high quality radar data is to avoid turbulent conditions. This is usually the case during night or cloudy but stable weather conditions (Caduff, Schlunegger, et al., 2015). During June 29th, 2021 and July 14th, 2021 the weather was mixed but basically windy and cloudy. Except for the windy periods, during which the GPRI was actually partially unable to make measurements, the weather conditions were rather favorable. When analyzing the raw data, it was noticed that there were some larger gaps (which are shown very clearly in figure 4) in the measurements, due to the wind. Thus, the data are narrowed down to the period from June 29th, 2021 20:00:01 to July 3rd, 2021 11:38:01.

Furthermore, with too low magnitude the difference between noise and real signal cannot be detected. Thus, azimuth lines as well as single pixels over the selected time were excluded from the analysis if their average magnitude was below a minimum threshold which was determined by trial and error.

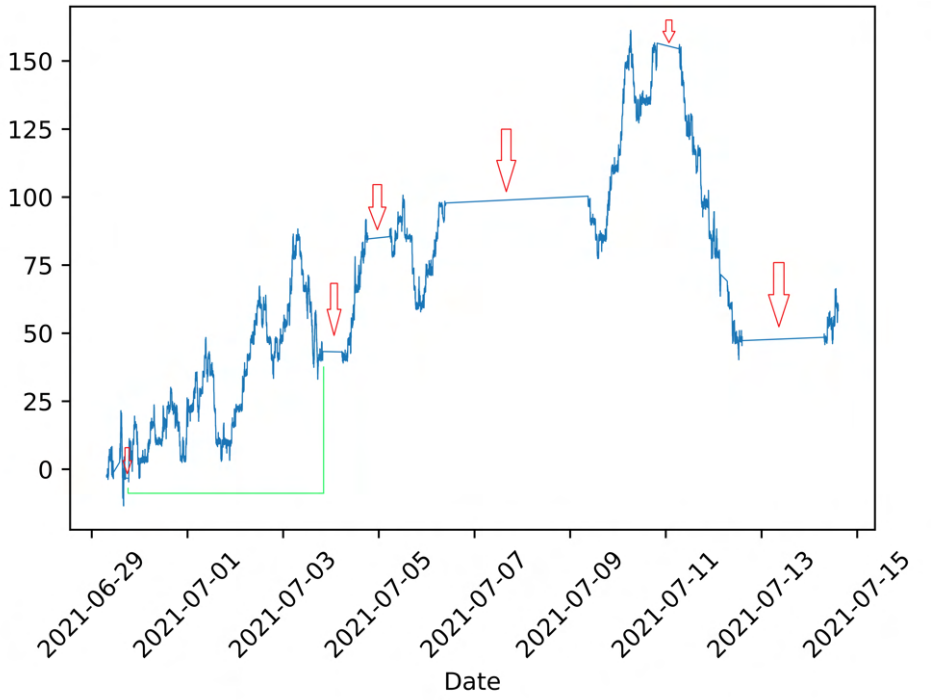

Figure 4: Illustration of the phase over the whole time period. Thereby larger gaps are recognizable which are marked with red arrows. The used time period is drawn in light green.

2.3.1.2 Time interval

A known difficulty of this master thesis was dealing with the large amount of data. An easy way to reduce the amount of data and thus shorten the calculation time is not to consider every measurement. The algorithm was tested by taking every sample, every second, every 10th and every 30th sample, which results in the following time intervals: 2min, 4min, 20min and 60min.

2.3.1.3 Meteo data

One of the most accurate approaches would be to detect and correct the atmospheric disturbance based on its originators, which include solar radiation, water vapor content, temperature and air pressure. However, it was determined that atmospheric disturbances vary over a very small area (Zebker, Rosen, and Hensley, 1997).

Obtaining data of this scale is not realistic, even if the meteo data availability is very high in Switzerland. The Federal Office of Meteorology and Climatology MeteoSwiss monitors around 300 measuring stations (*Data availability - MeteoSwiss* n.d.). Figure 5 shows the measuring stations around the study area. There is the station 'Gornergrat' and 'Monte

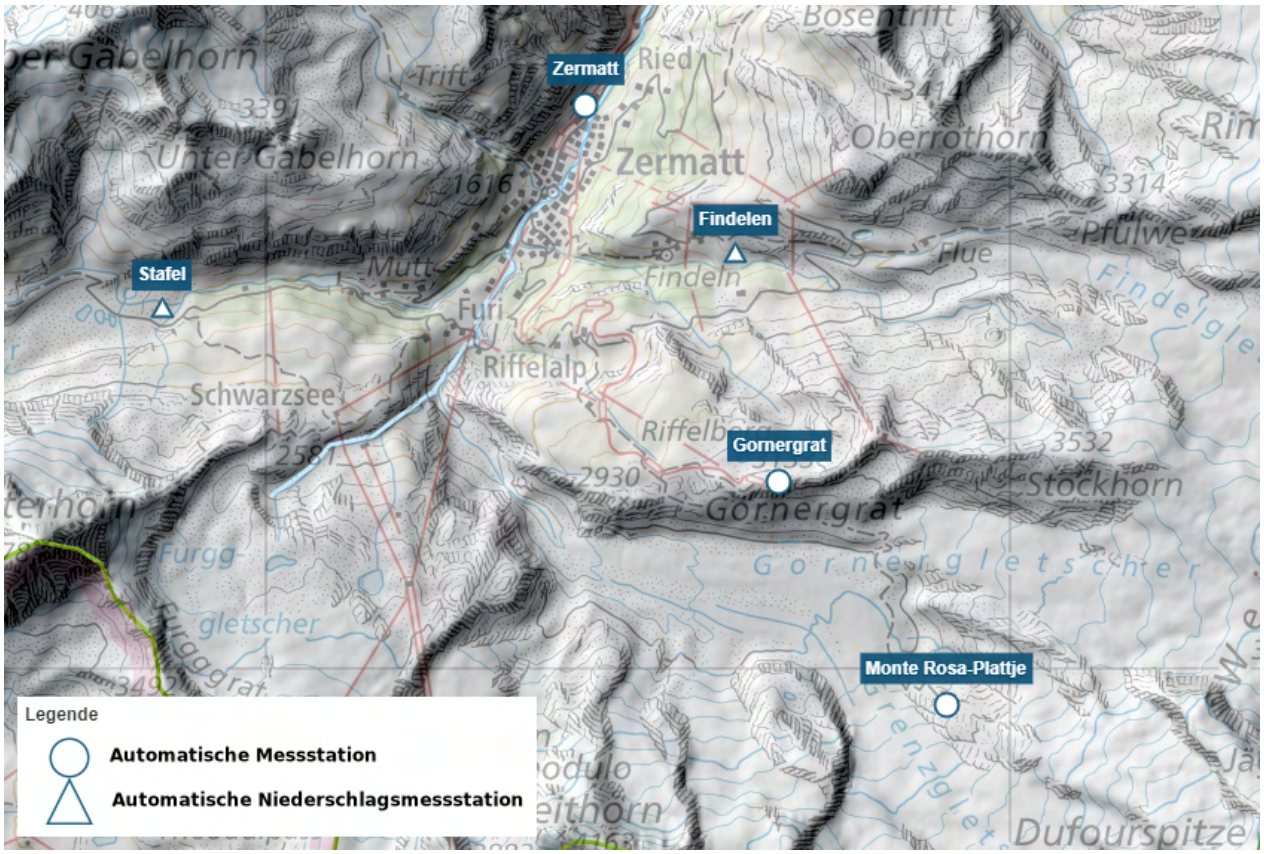

Figure 5: Measuring stations from MeteoSwiss around Gorner Glacier (Legend: ◯ automatic measuring station; △ automatic precipitation measuring station) (*Data availability - MeteoSwiss* n.d.).

Rosa-Plattje', which would provide most suitable data but unfortunately, the atmospheric perturbations show even smaller-scale patterns.

2.3.2 2nd algorithm - the adaptive filter approach

Goldstein and C. L. Werner (1998) developed a adaptive filtering algorithm, a low-pass filtering method, which smoothes the intensity of Fourier-transformed samples in overlapped interferogram patches. The phase noise is significantly reduced and therefore en improvement of measurement accuracy as well as phase unwrapping is expected. This approach of an adaptive filter GAMMA uses for their radar algorithms.

Andrea Kneib-Walter from the Institute of Glaciology and Geomorphodynamics at the University of Zurich computed the adaptive filtered (adf) interferograms for this thesis by using the Gamma software. The process to get the adf filtered interferograms consists of four steps: (1) Multi-looking to generate images with lower speckle and increased image quality. (2) Computation of interferograms to get the phase shift. (3) Adaptive filtering to

reduce the phase noise i.e. atmospheric disturbance. (4) unwrapping the phase shift and compute velocity of the movement. From these unwrapped interferograms, the flow velocity of the Gorner Glacier could then be calculated through the phase change similar to the first algorithm by the following formula:

$$v = \frac{\sum \left(p \cdot \frac{\frac{w}{2}}{2\pi} \right)}{t} \cdot 3600 \cdot 24 \tag{5}$$

Where p is the phase shift over two measurements, w is the transmitted and received wavelenghth from the GPRI and t is the time in seconds from the first to the last measurement. We get again v as the velocity in meter per day.

2.4 Data

2.4.1 GPRI data

In Summer 2021 from June 29th, 2021 to July 14th, 2021 data were collected at Gorner Glacier with a GPRI by a team of the Glaciology and Geomorphodynamics group of the University of Zurich. The GPRI was located at 45°57'29.5" N 7°48'44.0" E. In Figure 6 the location is marked on a section of a map (a) from SwissTopo and on a photograph (b) from Gorner Glacier. The measurements started on June 29th, 2021 at 07:27.44 and ended on July 14th, 2021 at 14:30.50 while a measurement was taken every two minutes. This measurement campaign resulted in 6316 measurements over this time period.

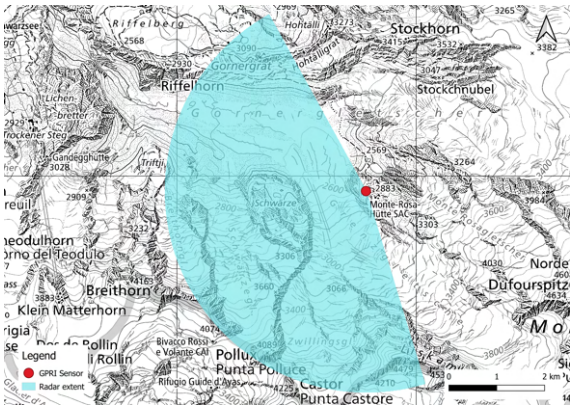

(a) GPS position of the GPRI (red dot) and the radar extent (cyan semicircle) on a section of a map from swiss topo.

(b) Position of the GPRI on a photograph of Gorner Glacier from M. Huss.

Figure 6: Position of the GPRI based on a map and a photograph

The data are stored in SLC products for each lower and upper antenna measurement separately where each image pixel is represented by a complex (I and Q) value and therefore contains both amplitude and phase information. Figure 7 shows an example of the intensity image of the GPRI measurement from June 29th, 2021 at 07:27.44.

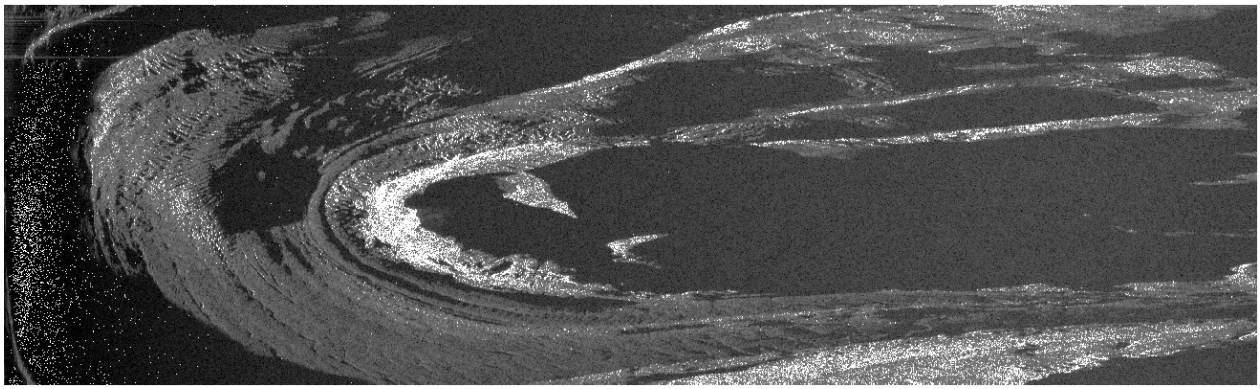

Figure 7: Intensity image of the GPRI measurement from June 29th, 2021 at 07:27.44.

2.4.2 UAV photogrammetry data

In the same time period of the GPRI measurements, UAV flights were conducted to get high resolution photogrammetry images. One flight per day was planned, due to the weather only on 11 out of 14 days were suitable flight conditions. On July 7th, 8th, 12th and 13th, 2021 no photogrammetry data are available. For this thesis the processed photogrammetry images and digital elevation models (DEM) were provided. Figure 8 shows an example of a modelled DEM of one flight, while on figure 18 the corresponding orthomosaic is depicted.

These high-resolution images serve as control data for the atmosphere-corrected and modeled velocities of the GPRI data. In order to calculate the flow velocity of the ice, prominent lines or points were traced across the DEMs and orthomosaics. The movement was calculated by the changed location and the corresponding change in the coordinates. For illustration, Figure 9 shows a control point moving across the flights. In this case, a very clear edge of a crevasse, which can be seen as a clear line in the DEM, was used as a control point. All control points and the corresponding coordinates are documented in the results section.

The velocity v of a control point n is given by the covered distance over time:

$$v_n = \frac{\sqrt{(y_m - y_{(m-1)}) + (x_m - x_{(m-1)})}}{t_m - t_{(m-1)}} \tag{6}$$

While

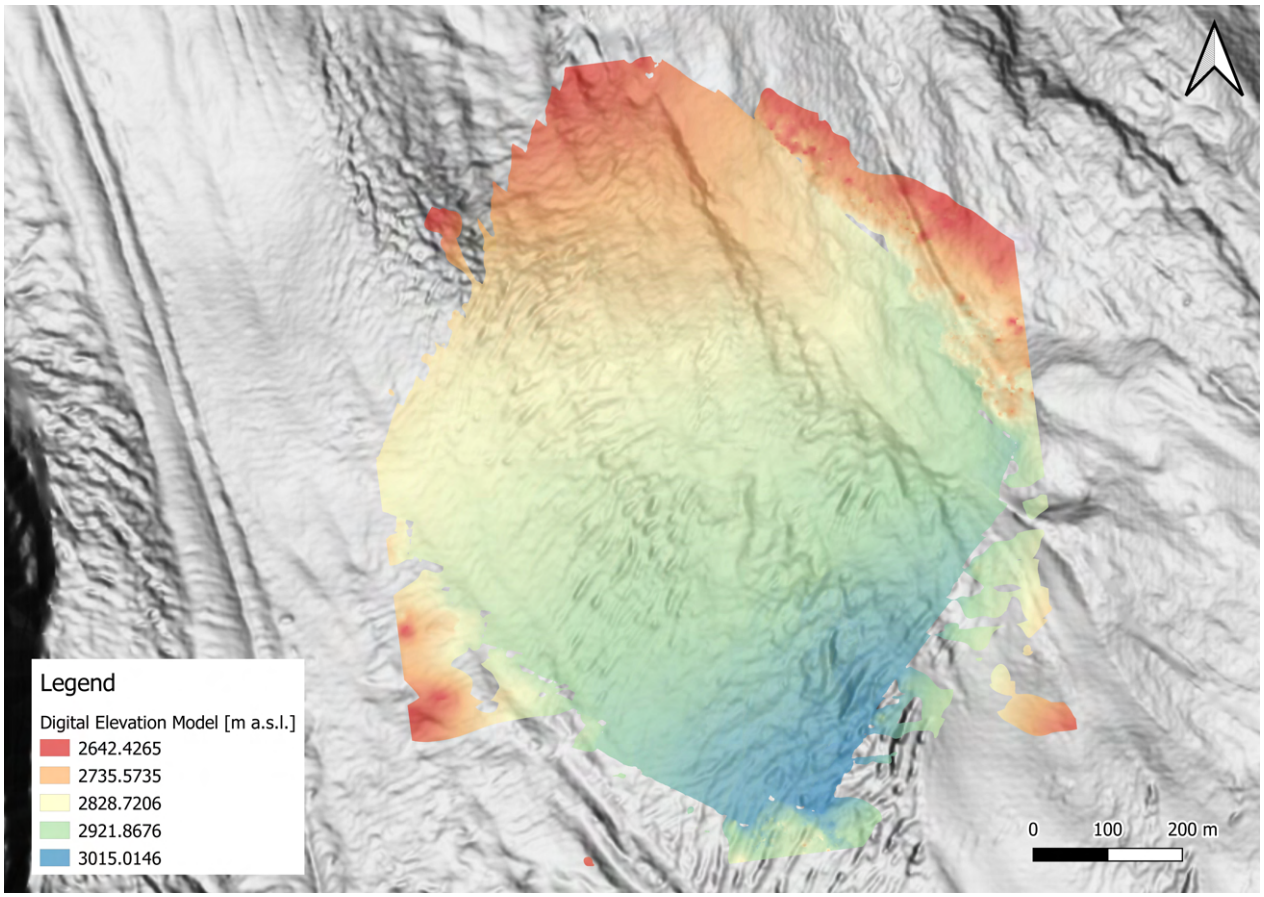

Figure 8: Processed DEM from June 30th, 2021 based on UAV data.

v_n = the resulting velocity in [m/s],

y_m, $y_{(m-1)}$, x_m and $x_{(m-1)}$ = the X und Y coordinates of one measurement and the one before. By using Pythagoras one can calculate the distance in [m] of the movement between two flights and finally,

t_m and $t_{(m-1)}$ = the time stamps of the flights to calculate the time in seconds [s] between two measurements.

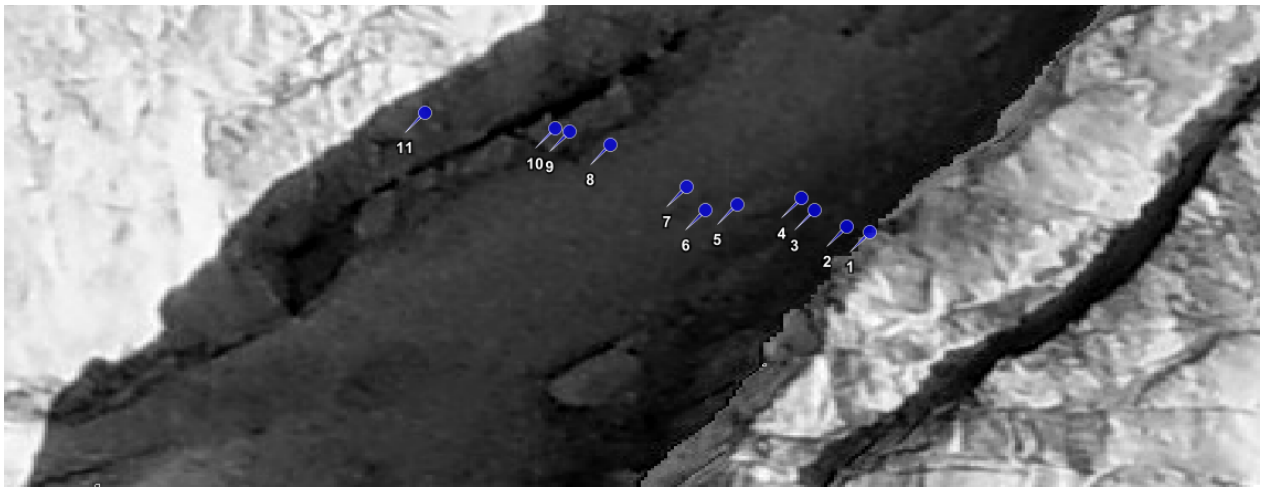

Figure 9: Movement of one control point from June 29th, 2021 to July 14th, 2021. This image covers a length of approx. 15 metres.

3 Results

The focus of the results is on the first algorithm. The results are described in principle and a specific focus is placed on individual optimization possibilities. Daytime and nighttime measurements are compared and the behavior when the time interval between the recordings is increased. Subsequently, the results from the second algorithm and the control points from the UAV data are described.

3.1 1st algorithm

The results of the first algorithm are particularly interesting because this approach has not been used much before. The resulting speed map shows (figure 10) a realistic picture. The velocities lie between $-0.122\,\mathrm{m/d}$ and $0.84\,\mathrm{m/d}$, while the majority of pixels have a modeled velocity between $-0.1\,\mathrm{m/d}$ and $0.05\,\mathrm{m/d}$. A positive result means that the movement is towards, whereas a negative result means a movement away from the sensor.

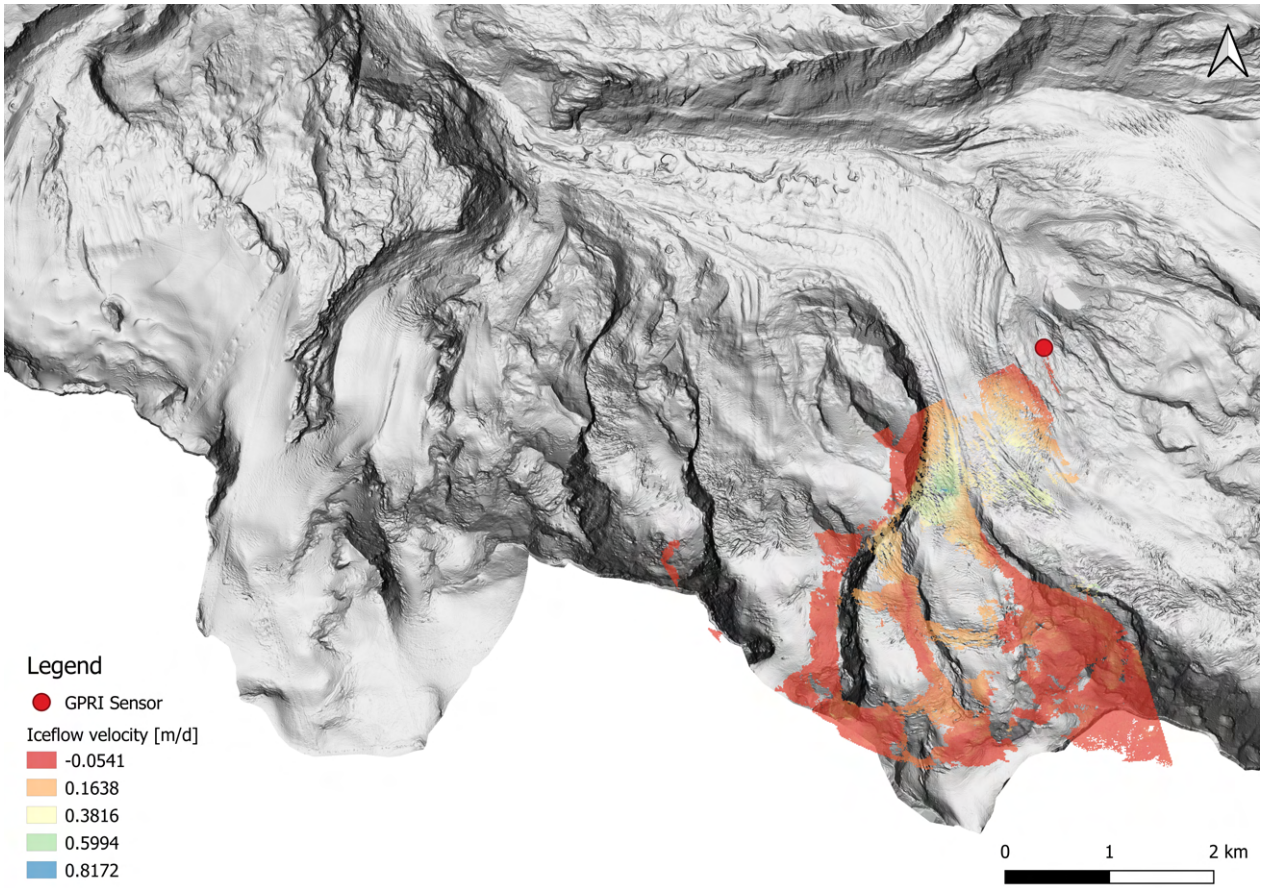

Figure 10: Geocoded velocity map corrected for atmospheric disturbance by algorithm 1 of 800 azimuth lines over Gorner Glacier and surrounding areas.

3.1.1 General results

To test the effectiveness of the correction for atmospheric disturbance, individual range samples were examined. In particular, we concentrated on the part of the glacier for which the UAV data are available, otherwise no validation with the control points can take place. Comparing the resulting velocities of these five range samples it shows the following results which are summarized in table 1.

Table 1: Resulting ice flow velocity [m/d] at the position of the five tracked control points corrected by atmospheric disturbance by algorithm 1.

Point No.	azimuth line / range sample	avg. velocity [m/d]	
		uncorrected	corrected
1	517 / 891	0.27	0.25
2	794 / 663	0.19	0.18
3	446 / 535	0.09	0.09
4	404 / 1169	0.37	0.37
5	327 / 1082	0.31	0.31

The difference between the corrected and the uncorrected modelled velocities are hardly noticeable. To better understand how the algorithm works, the phases are investigated in more detail. On the one hand, the phase changes of the control points were studied, as well as range samples on the same azimuth line. On the raw phase nothing is recognizable due to the phase wrapping. However, as soon as the phase is unwrapped (Figure 11(a)), a clear trend is visible, also the noise on the radar signal are clearly observable. In figure 11(a) it is also visible that the corrected phase shows a clear smoothing compared to the uncorrected phase. Additionally, it's worth mentioning that the corrected phase has a smaller slope.

A main assumption is that the atmospheric disturbance behaves similarly over an azimuth line. Thus, the unwrapped and detrended phase of different range samples on an azimuth line was investigated. It is very clear that the noise has a large variability (figure 12).

3.1.2 Difference between day and night measurements

As already mentioned in the methods section, there is the least interference radar recordings at night and in cloudy weather. In July, the sun rises in Switzerland at about 05:30 a.m. and sets at 09:30 p.m. At night from July 1st, 2021 to July 2nd, 2021 and from July 2nd, 2021 to July 3rd, 2021 the wind was too strong, such that the GPRI could not take any measurements from 8:00 p.m. to 06:00 a.m. and from 19:00 p.m. to 06:00 a.m. respectively. The following nights were examined in more detail:

- 29./30.06.2021

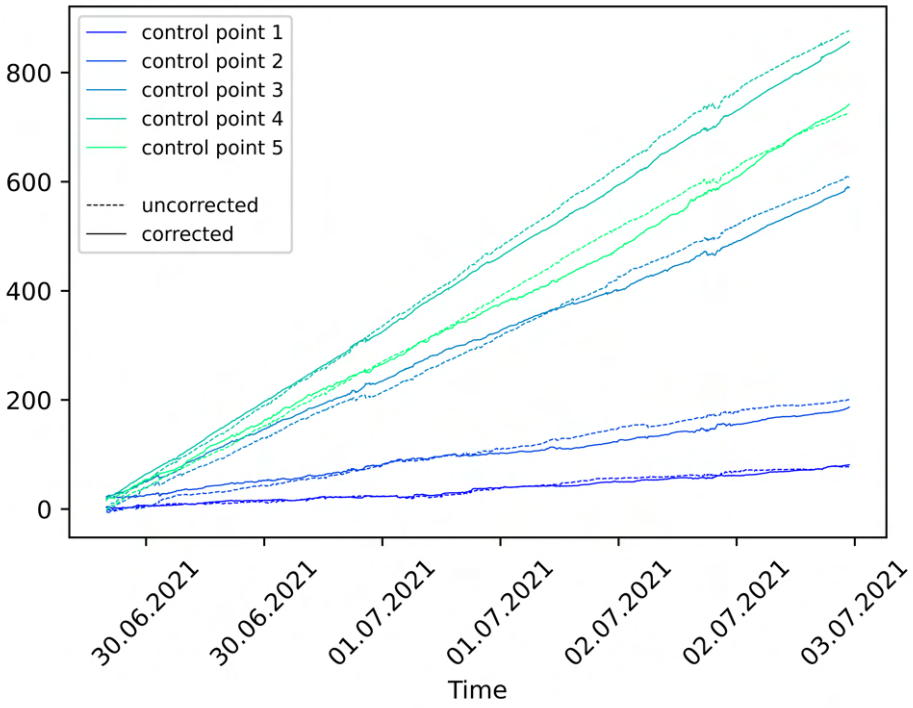

(a) Uncorrected and corrected and both unwrapped phase.

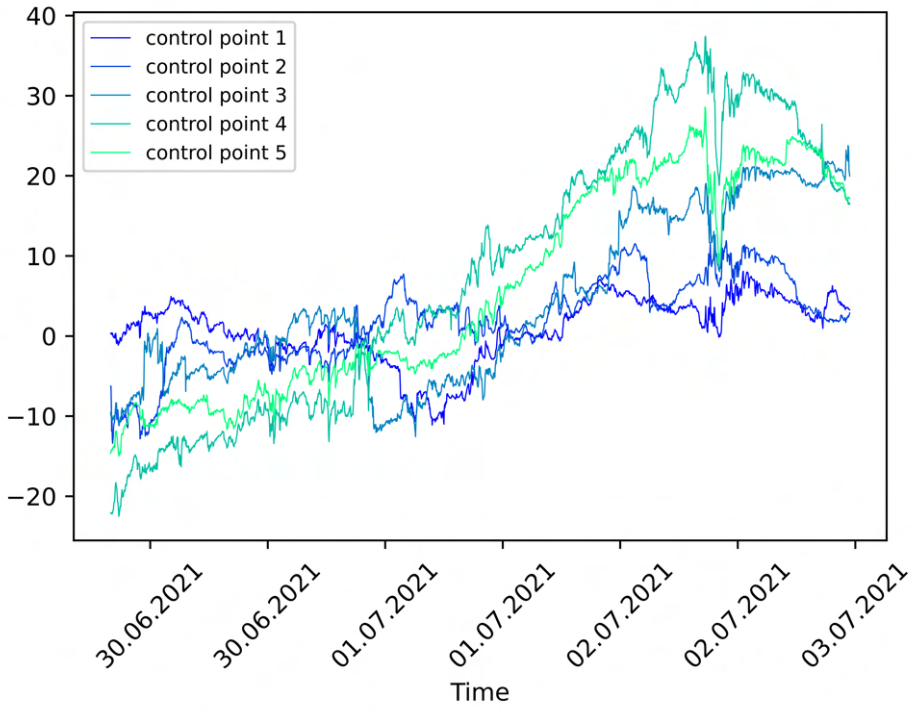

(b) Unwrapped and detrended phase (the expected noise).

Figure 11: Phase of the five control points.

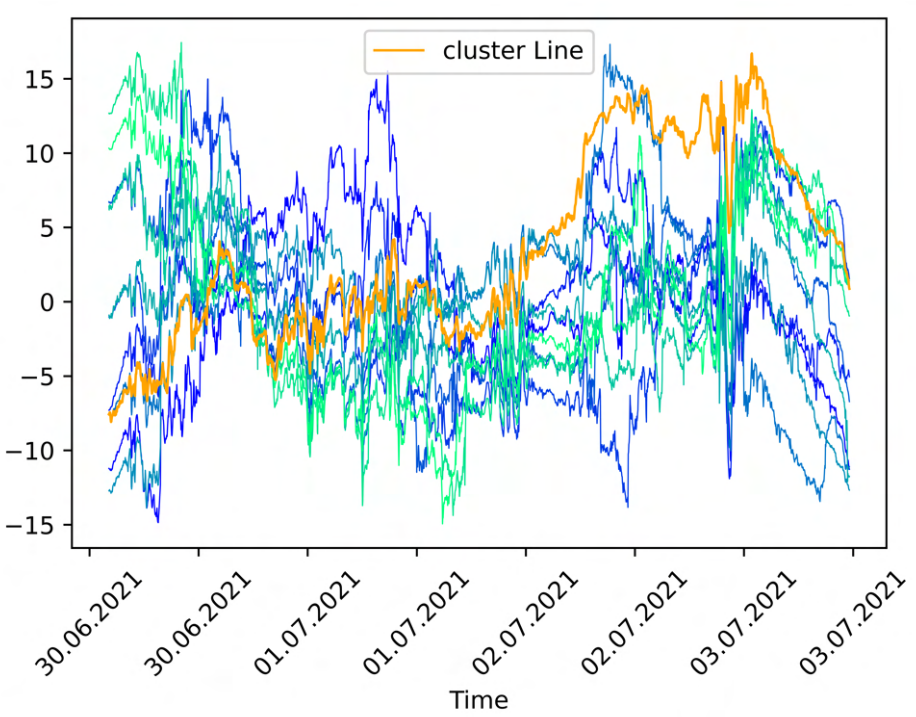

Figure 12: Unwrapped and detrended phase of 10 different range samples (green to blue colors) and the clustered atmospheric noise (orange) of one azimuth line.

- 30.06./01.07.2021
- 01./02.07.2021
- 02./03.07.2021
- 05./06.07.2021

Lower deflections in the phase change would be expected at night. If the radar signal were sensitive to temperature and/or pressure, the samples should show a similar pattern at night. Unfortunately, neither is the case. Figure 13 shows the pattern of the unwrapped and detrended phase of five different range samples during the mentioned nights. There is no time period which shows a lower noise persistently and consistently over all studied nights. Also the pattern of the noise also varies differently each night.

3.1.3 Adjustments of the time interval

72 megabytes are required for a radar measurement in the SLC format of the GPRI. During the two weeks of measurement on the Gorner Glacier, 12′632 measurements were made, resulting in a storage amount of 880 gigabytes. Working with such a large amount of data

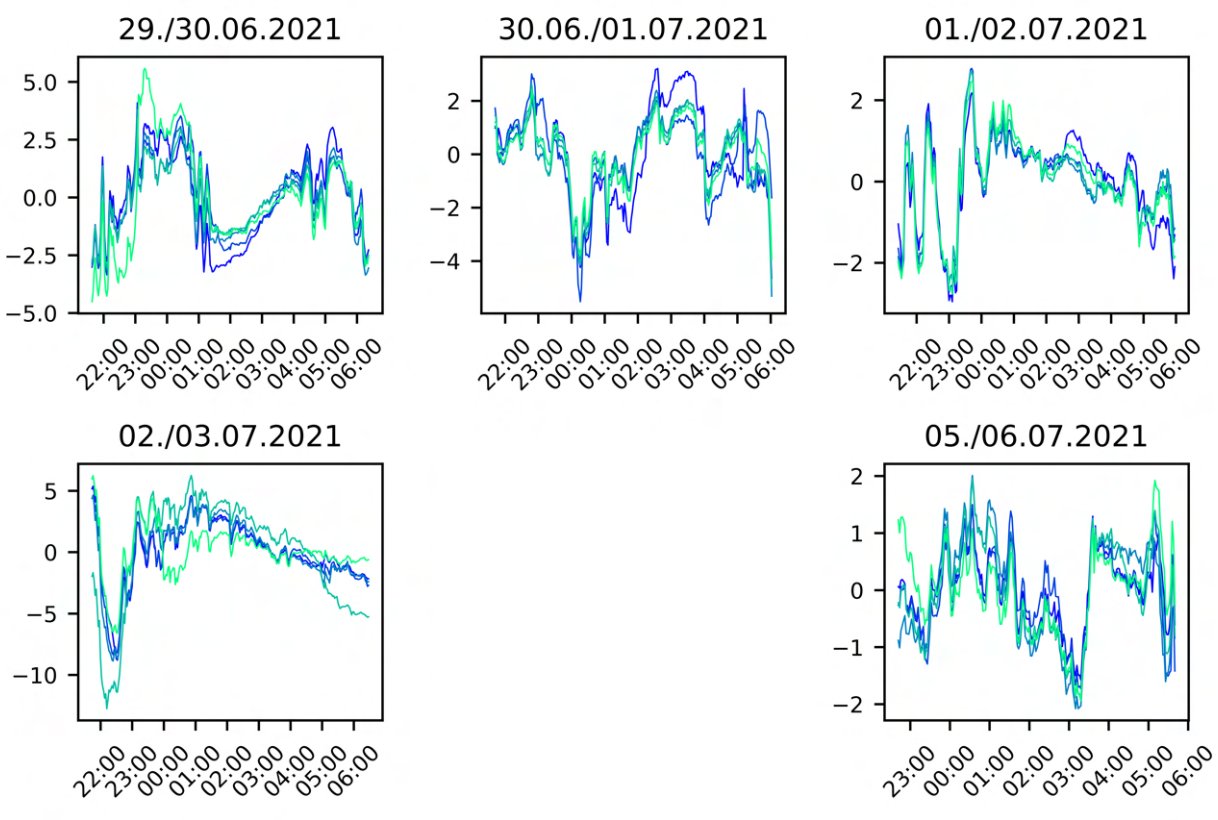

Figure 13: Plot of unwrapped and detrended (noise) phase range samples over night.

is challenging and the processing time is very high unless very performant servers are available. Therefore, during this work, the question arose whether a measurement interval of two minutes is really necessary, and how a larger time interval would affect the results. In order to find an answer for these questions, a time interval of 2 min, 4 min, 20 min and 60 min was used and individual range samples were compared with each other. Figure 14 shows the unwrapped phase of two range samples with the different time intervals. It is very clear that the trend flattens strongly with increasing time interval. Also worth noting is that the difference between each measurement and every second measurement is very small.

The time for processing 200 azimuth lines was measured for all time intervals. Table 2 lists the results and significant differences can be seen. While the processing of all azimuth lines takes 11.73 min, the process takes only 7.26 min for every thirtieth measurement, which corresponds to a time saving of just under 40%.

3.2 2nd algorithm

The second approach represents an often used method to correct atmospheric disturbance in radar images. An adaptive filter is used to eliminate unwanted noise on the radar signal. In

(a) Azimuth line 700 and range sample 600.

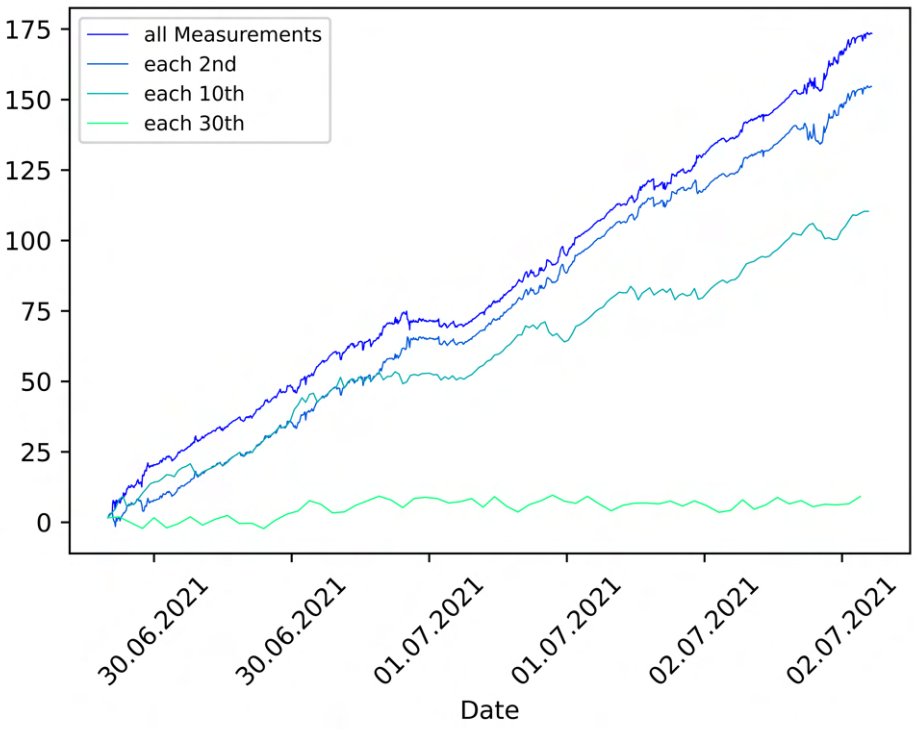

(b) Azimuth line 795 and range sample 870.

Figure 14: Lineup of unwrapped phases with different time intervals of taken measurements.

Table 2: Results of the time measurement for the processing of 200 azimuth lines with different time intervals.

Time interval [min]	Measured time [min]	Deviation [%] from the original time interval
2	11.73	0.00
4	8.50	21.37
20	9.23	27.73
60	7.26	39.29

a first step, multi look images (MLI) were generated out of the original radar measurements. Figure 15 shows the difference between (a) the original radar image and (b) the multi look image (MLI). By a down sampling factor of 3 in range direction almost rectangular pixels have been achieved. Areas of 0.100008 m in azimuth 2.249736 m in range direction can now be differentiated. Additionally, a better quality should be achieved by the aggregation and averaging of pixels and thus reduction of noise.

Table 3: Resulting ice flow velocity [m/d] at the position of the five tracked control points corrected by atmospheric disturbance by algorithm 2.

Point No.	azimuth line / range sample	avg. velocity [m/d] corrected
1	517 / 297	-0.28
2	794 / 221	-0.04
3	446 / 178	-0.09
4	404 / 390	-0.38
5	327 / 361	-0.33

The MLIs are the basis for the calculation of the interferograms which are calculated afterwards. Figure 16 shows the interferograms between July 4th, 2021 at 06:16:02 and 06:18:02 while (a) is the raw interferogram and (b) the adaptive filtered interferogram respectively. Striking are the two stripes in the upper part of the images, which are not corrected but rather enhanced in the adaptive filtered (adf) interferogram. In general, the adf interferograms look smoothed, but not really corrected for the atmospheric disturbance.

If we look at the resulting velocities of the five control points in table 3 it is conspicuous that all results are in the negative range, which means that all pixels move away from the GPRI sensor. The overall velocity ranges between -0.77 m/d and 0.17 m/d while the majority of pixels have a modeled velocity between -0.1 m/d and 0.1 m/d. Figure 17 shows the resulting geocoded velocity map corrected my the second algorithm.

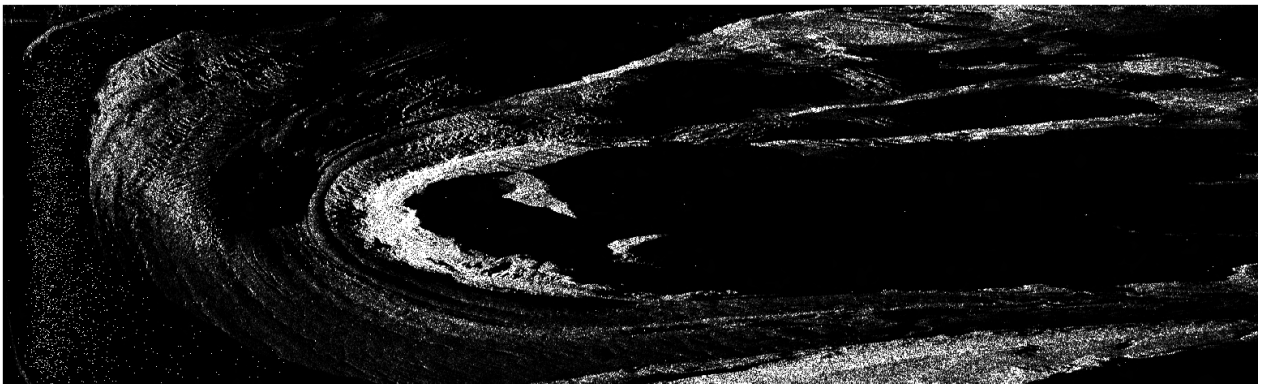

(a) Original intensity image in radar geometry

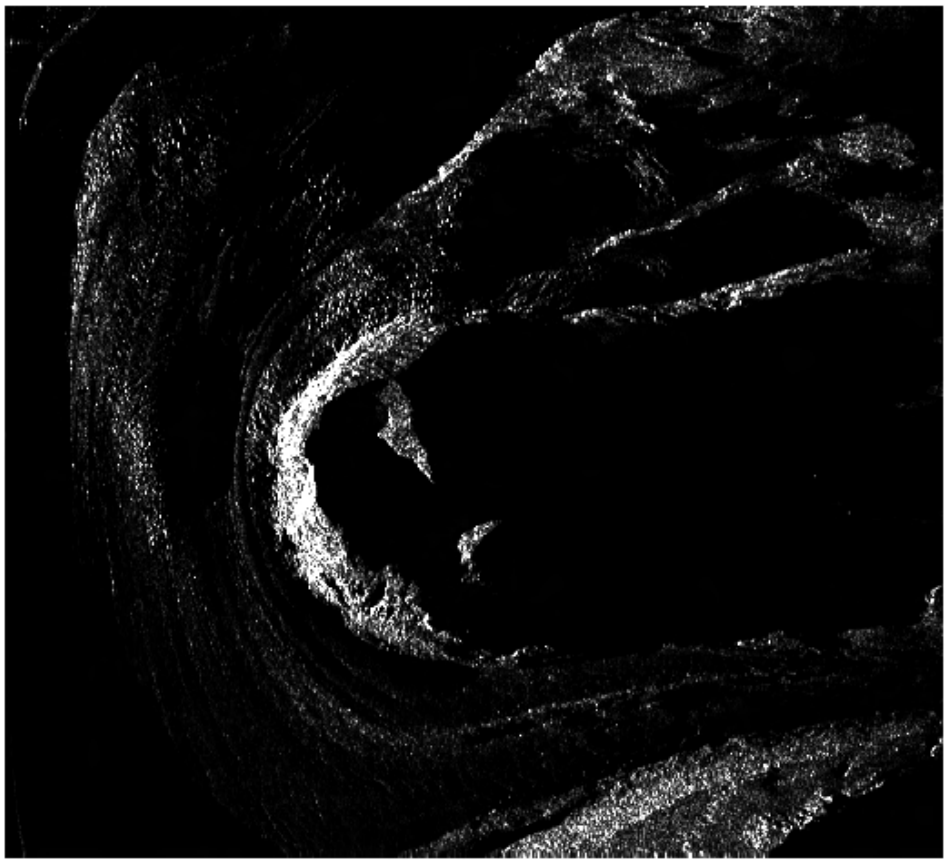

(b) Multi look image in radar geometry

Figure 15: Radar images from July 4th, 2021 at 06:16:02

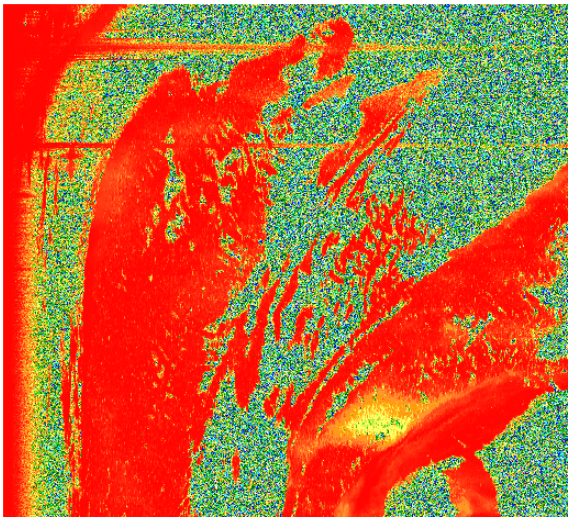

(a) Raw interferogram

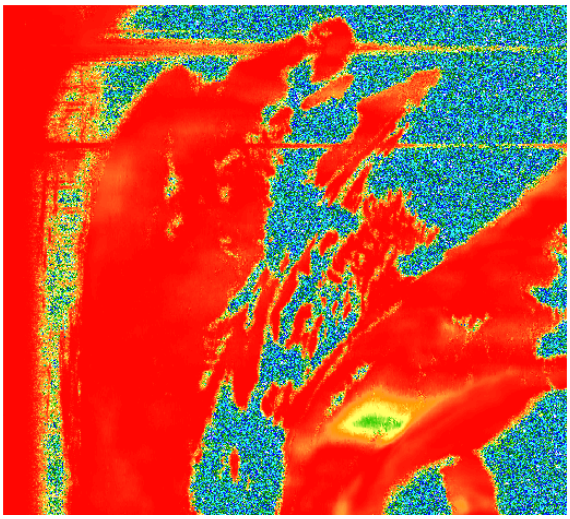

(b) adf interferogram

Figure 16: Interferograms between July 4th, 2021 at 06:16:02 and 06:18:02

3.3 UAV control points

In order for the results of the two atmospheric correction algorithms based on GPRI data to be tested with independent data, UAV imagery was used to track five control points over the same time period. The results are shown in Table 4. The points were selected to cover all areas of the recorded glacier. Figure 18 shows the distribution of control points on the first image taken on July 30, 2021.

Table 4: Resulting movement and velocity of five tracked control points.

Point No.	Start Lat/Lon End Lat/Lon	avg. Movement [m]	avg. Velocity [m/d]
1	45.95290489/7.80676177 45.95288197/7.80676852	2.55	0.85
2	45.95448513/7.80583233 45.95446563/7.80583827	2.17	0.72
3	45.95456637/7.80945274 45.9545466/7.80945688	2.20	0.73
4	45.95057711/7.80725749 45.95055145/7.80727184	2.85	0.95
5	45.95027132/7.80983465 45.95025399/7.8098486	1.93	0.64

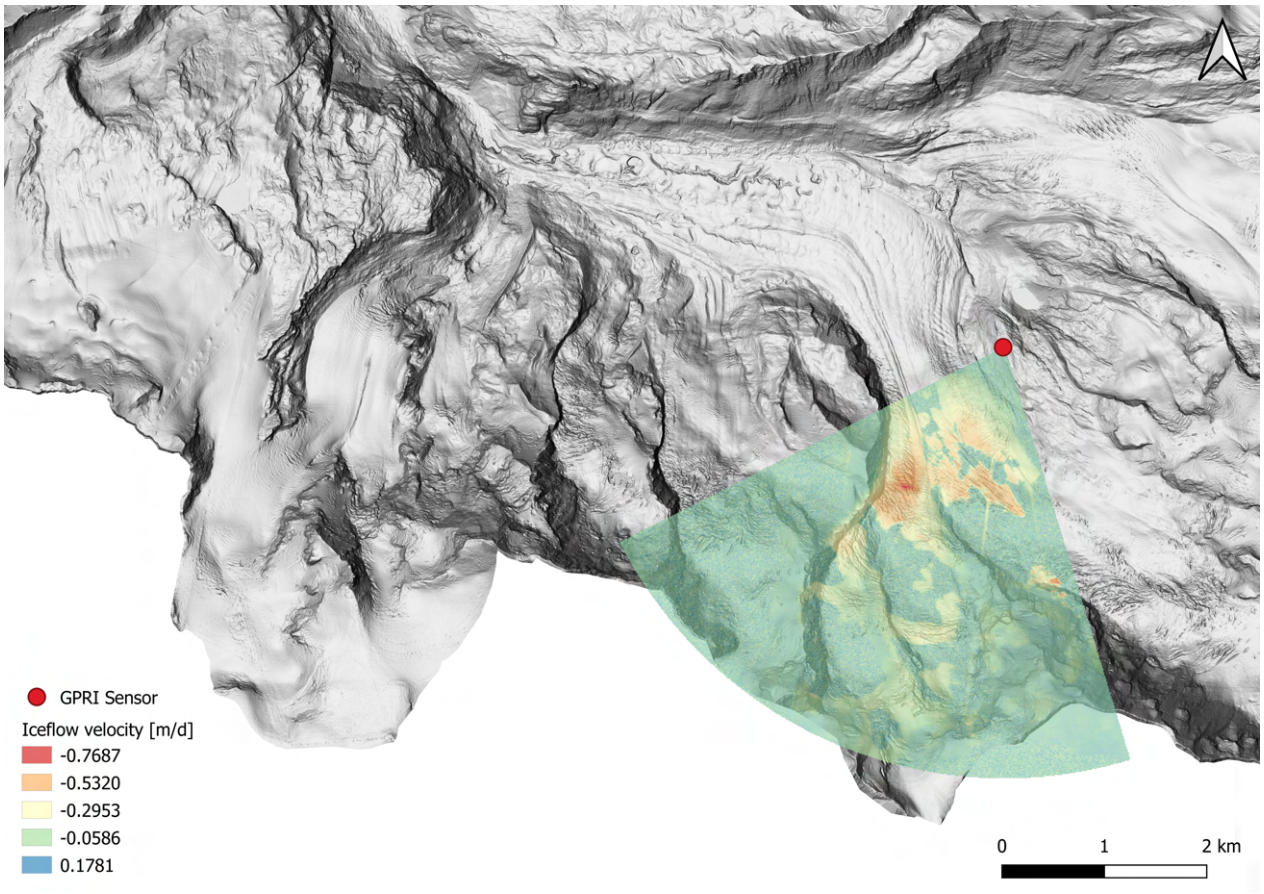

Figure 17: Geocoded velocity map corrected for atmospheric disturbance by algorithm 1 of 800 azimuth lines over Gorner Glacier and surrounding areas.

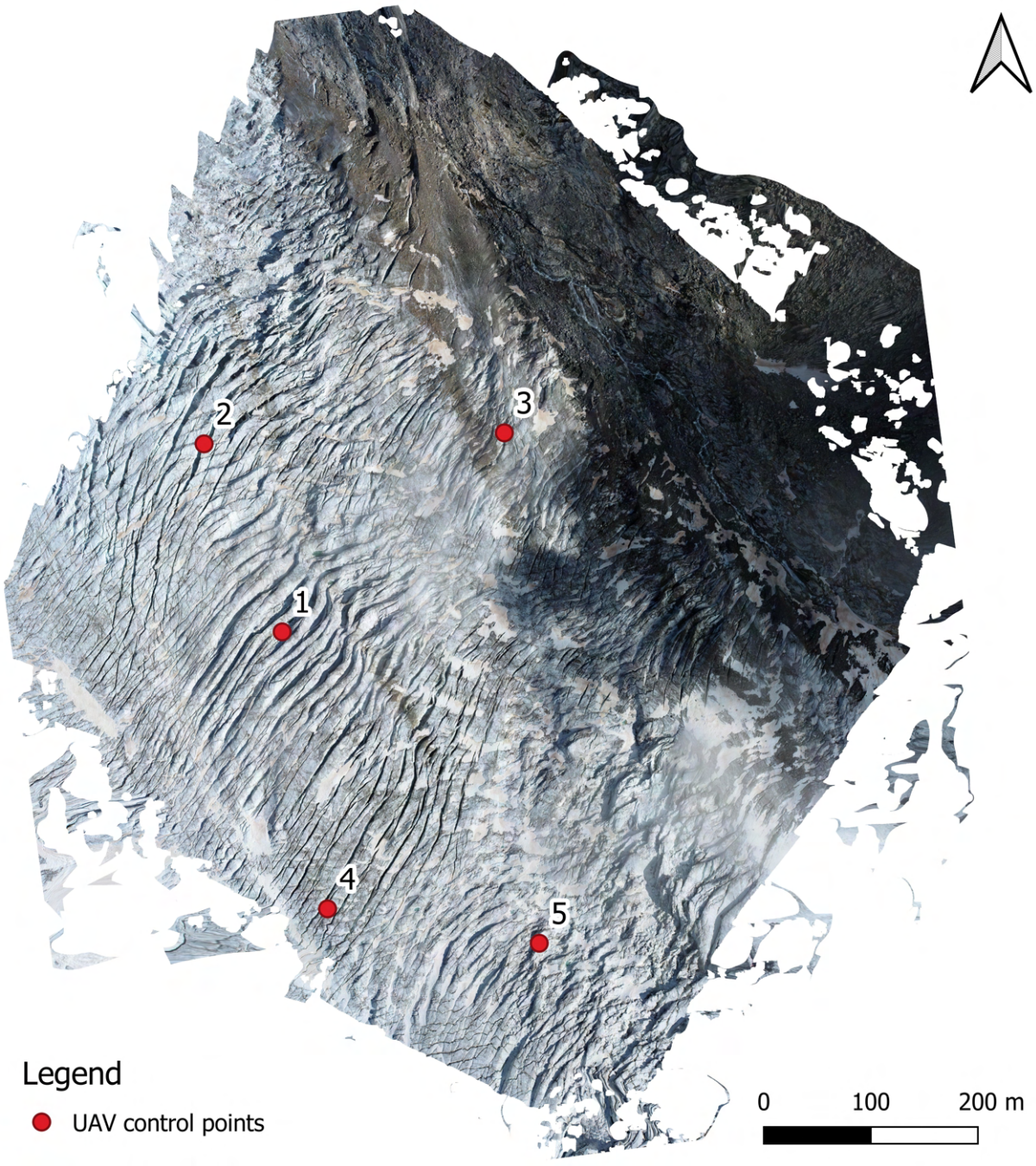

Figure 18: Tracked control points on the orthomosaic image from June 30th, 2021.

4 Discussion

The results offer a wide variety of possibilities to be investigated. In particular, this work attempted to determine if the two studied algorithms can be used to correct the atmospheric disturbance on the radar images. To answer the research question, in the following subsections the results are getting compared with each other, open issues are addressed and ideas for further developments and investigations are explained.

4.1 Comparison between algorithm 1 and algorithm 2

To answer the research questions whether the two algorithms are able to correct the radar signal for atmospheric disturbance enough to calculate the ice flow velocity and if one of the two algorithms works better, the results from both algorithms are compared with the control points from UAV and also with each other respectively. In a first step, only the velocities are compared, the direction is ignored. Therefore, in this sections the absolute values of the results are considered in this section.

The results of algorithm 1 and 2 are based on the same data, so it is evident that the results show rather small differences. The differences are between 0.06 m/d and 0.38 m/d. The detailed calculation of the differences can be found Table 5. Looking at Figure 19, it is apparent that control points 1 and 5 have the smallest differences, although it is interesting to note that control point 1 was modeled higher by algorithm 1 than by algorithm 2 and vice versa for control point 5.

Table 5: Differences [m/d] between the velocities of algorithm 1, algorithm 2 and the UAV control points respectively.

Point No.	Algorithm 1 vs. Algorithm 2	Algorithm 1 vs. UAV	Algorithm 2 vs. UAV
1	0.06	0.36	0.30
2	0.19	0.35	0.54
3	0.28	0.46	0.18
4	0.37	0.33	0.70
5	0.12	0.16	0.29

Control point 3 is located at the border of the glacier near the moraine on the sensor side. Since a glacier flows faster in the middle than at the borders, a slower ice flow velocity is expected for control point 3 as for the points which are located in the middle of the glacier. This assumption was confirmed by algorithm 1 but not for algorithm 2.

Points 2 and 4 are estimated significantly lower by Algorithm 2 than by Algorithm 1. However, if we look at figure 17 more closely, it can be determined that these two points are located in an area with a lack of coherence. A lack of coherence is caused by different backscatter behavior between two acquisitions. By disordered movements of the individual scatterers (in this case e.g. the atmosphere) between two images, the backscattering behavior can be changed significantly, so that the phase differences are random (decorrelated) and consequently not interpretable (Caduff, Strozzi, and Wiesmann, 2013). A comparison of these two points therefore is meaningless.

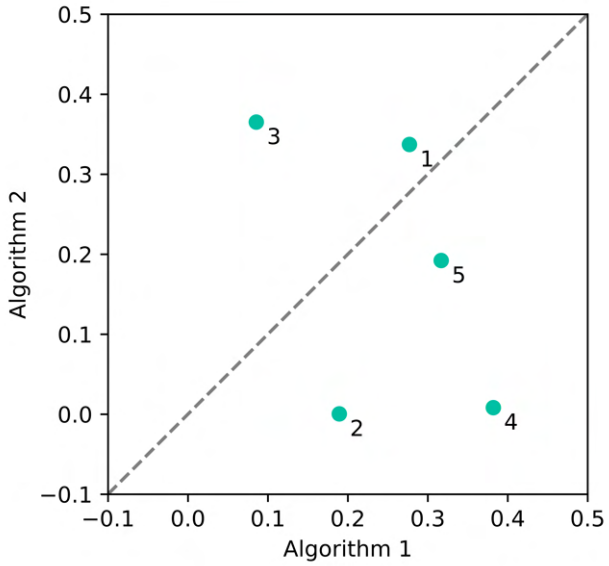

Figure 19: Comparison of the resulting velocities from algorithm 1 and algorithm 2 of the five control points.

4.2 Validation with the control points from UAV photogrammetry

It can be seen from figure 20 that the calculated velocities from the UAV data are significantly higher than the results of the two studied algorithms, which are based on the GPRI data. There are differences of 0.16 m/d to 0.46 m/d for algorithm 1 and from 0.18 m/d to 0.70 m/d for algorithm 2 respectively in comparison with the control points.

The magnitude of the calculated velocities of the ice flow of the Gorner Glacier by UAV data could be confirmed by Benoit et al. (2019). In his study, the ice flow velocity of the Gorner Glacier was also determined with UAV and measured velocities of 0.4 m/d to 0.75 m/d in our investigated area.

Here it should be mentioned that surface changes are measured only as line-of-sight displacements. This means that only the degree to which a point moved toward or away from the

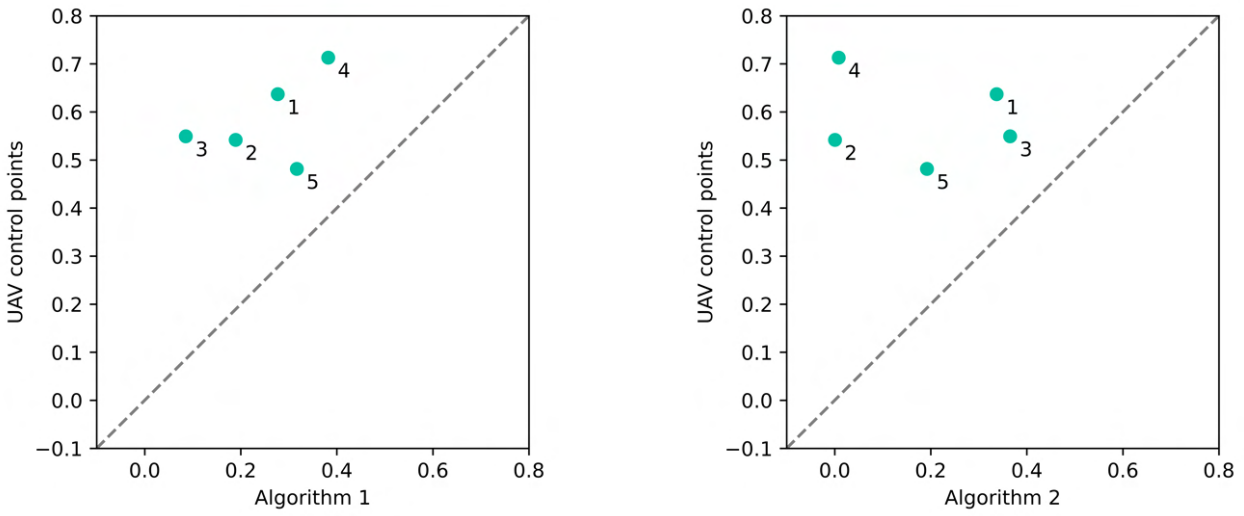

(a) Algorithm 1 vs. UAV control points

(b) Algorithm 2 vs. UAV control points

Figure 20: Comparison of the resulting velocities from algorithm 1 and the UAV data of the five control points.

radar sensor look direction can be measured (Lillesand, Kiefer, and Chipman, 2015; Caduff, Strozzi, and Wiesmann, 2013). The area covered by the UAV flights is pretty much parallel to the sensor and thus very inconvenient to obtain accurate measurements. This will be a reason why the results are consistently underestimated. Here a correction factor would be necessary depending on the angle to the sensor.

But at least for points 1, 2 and 4 it can be deduced that the velocities from algorithm 1 und the UAV data behave proportionally.

4.3 Correction of atmospheric disturbance

The focus of this thesis was the correction of atmospheric disturbance on the radar signal. After the results have been compared and interpreted, the actual process of atmospheric correction will now be examined in more detail in the following subsections especially for algorithm 1.

4.3.1 Clustering of the hypothetical atmospheric disturbance

The results show a large variation of the assumed disturbance (unwrapped and detrended phase) within one azimuth line. The approach to find a general pattern of atmospheric disturbance by clustering the unwrapped and detrended phase cannot be extensively confirmed. The corrected phase indeed shows a smoothing of the phase shift, but the resulting velocity varies only minimally in contrast to the uncorrected phase. Nevertheless, it can be stated

that the estimation of the velocity by the slope of the unwrapped phase has potential and should be investigated further, since by considering a longer time series and assuming uniform movement of the glacier, outliers due to faster and more irregular movements caused by circulating air above the ice can be excluded.

For further investigations one is recommend not to combine the disturbance over a whole azimuth line. It might work better to combine several azimuth lines over fewer range samples. Thus, for example, the air blobs could be assumed to have square shapes. Additionally, an often used approach is to estimate the disturbance over stable terrain (e.g. rock). This approach could well be included in algorithm 1.

Another but way more complex approach would be to track the air blobs via artificial intelligence and thus the possibility to directly and accurately correct the affected azimuth lines and range samples.

4.3.2 Selection of good and low noise data

The wind was strong during the recording time and repeatedly led to interruptions in the recordings. It would be interesting to investigate whether the wind causes the sensor to move and can thus lead to large phase changes. Since the estimation and correction of the atmospheric disturbance on the radar signal is very complex, it is worthwhile to pay attention to good weather conditions. But due to the high revisit time and the assumption that a glacier flows regularly, it is possible to make initial estimates of the flow velocities after short time.

4.3.3 Choice of time interval

The investigations have shown that the difference in the results does not show much change when increasing the time interval from 2 min to 4 min. With an increase to 20 min or 60 min, the phase shift flattens out significantly. In combination with the reduction in the required time for processing the data, it can be said that increasing the time interval to 4 minutes is worthwhile. But it should be mentioned that with the wavelength of 17.2 GHz from the GPRI, it is possible to correctly detect movements of a maximum of 8.72 mm between to acquisitions. Thus, to increase the time interval only applies to movements that do not exceed this value. This works well for an alpine glacier like Gorner Glacier. For a maritime glacier for example, a limit is already reached at a time interval of 2 minutes (Jouvet et al., 2020).

4.4 Identification of uncertainties and inaccuracies

Since the velocity of TRI of both algorithms is extracted after multiple assumptions and processing steps, the resulting velocities are only approximations of the real motion of the ice. The sources of these uncertainties and inaccuracies will be identified and discussed for both algorithms in the next paragraph.

First of all, the calculations were done in the radar geometry and only the final results were resampled and reprojected into the swiss coordinate system LV95 (EPSG: 2056). Thus, errors due to resampling are independent of the earlier processing steps and do not influence the final results.

The first algorithm makes some assumptions, resulting in a very simple model, but also introduces large uncertainties and inaccuracies. The assumptions are listed below:

- A maximum phase jump of 4 was defined for which a phase shift will be unwrapped.
- Only range samples with a minimum magnitude of 0.3 were used for the calculation. Determining a fixed value does not make much sense and could be determined more sensibly and individually.
- The disturbance on the radar signal is assumed to be the unwrapped and detrended phase.
- The disturbance is generalised with a cluster method and corrected equally over the entire time and over an azimuth line.
- The velocity of the glacier is equated to the trend of the phase shift.

Also the second algorithm contains multiple processing steps such as multi-looking, interferometric correlation calculation, phase unwrapping, thus the accuracy can be influenced by many factors. The multi-looking image processing has the advantage of reduced speckle noise and more or less quadratic pixels, but the disadvantage of a reduced range resolution due to the resampling in range direction.

Aditionally, it has been shown that in steep topography, altitude-dependent phase components may be present in the terrestrial radar data set. In steep mountainous terrain, like in our part of Gorner Glacier, atmospheric effects can contribute to localized but strong perturbations of the interferograms even for short observation times on the order of minutes. (Caduff, Schlunegger, et al., 2015).

5 Conclusion

The aim of this master thesis was to evaluate two different algorithms that allow for a correction of the atmospheric disturbances of the radar signal of a GPRI.

The central questions for this thesis were as follows:

RQ1 Can the atmospheric disturbance be corrected enough to calculate the glacier's flow rate plausibly?

RQ2 Can a significant difference be found between the two algorithms?

RQ3 If the second research question (RQ2) answered with yes, which of the two investigated algorithms is better suited for the correction of atmospheric disturbance?

After processing the data using the two algorithms and determining the flow velocities of the control points using UAV data, the actual analysis could begin. The differences between the modeled velocities with the GPRI data and the calculated control points are large, so that the research questions whether the algorithms for the correction of atmospheric disturbance work well enough to derive the ice flow velocity, must unfortunately be answered with no.

It must be mentioned, however, that this is not primarily due to the atmospheric correction. Actually, it was expected that the velocities would be too high because the air above the glacier moves significantly faster than the glacier itself. It could be clearly established that the atmospheric disturbance causes small deflections on the signal, which, however, do not significantly change the trend of the phase shift. This fact strongly supports the assumption that it is reasonable to observe the movement over a period of at least a few hours so that the trend can be clearly separated from the noise. Due to the very high revisit time, this can be implemented without any problems. Both algorithms based on GPRI data gave results in a similar range. Thus, neither algorithm is significantly better than the other. It was astonishing but also gratifying that the calculation of the flow velocity based on the UAV data could be confirmed by the paper of Benoit et al. (2019), although the approach to the calculation by manual tracking of well visible shapes did not promise much accuracy.

However, the close examination of the data and the two algorithms has opened up many more possibilities and ideas with which the calculation of ice flow velocity with GPRI could be useful.

In order to improve the results based on the existing data, it would be very interesting to figure out whether a generally valid correction factor can be determined which corrects for the unfavourable location of the GPRI sensor. For next studies with terrestrial radar, the

sensor should be placed in a location where the ice flows more direct towards or away the radar look direction. In the case for Gorner Glacier, this would be possible, for example, from the Gornergrat observatory, which would also be well accessible. Additionally, one should pay attention to a favourable time window for the radar measurements. This means either at night or when it is cloudy. The analysis of a tilt sensor would be useful to exclude or correct for distortions due to the movement of the sensor as a result of wind.

A combination of different approaches would be interesting to investigate. Just the combination of multi-looking and the adaptive filter and calculating the speed based on the trend of the phase shift sounds promising. In addition, stationary pixels should be investigated for a better estimation of the atmospheric disturbance and especially a differentiation from other noise. More recently, artificial intelligence has been applied in scientific research. Ouyed Hernandez et al. (2020) investigated an approach to improve the modelling of atmospheric motion using feature tracking. Should such an approach become established, it would also be exciting for tracking air blobs over a glacier.

In conclusion, it can be stated that the advantages of GPRI, with its high revisit time, incredible spatial resolution and the easy installation of the sensor, outweigh the disadvantages and challenges, so further investigation is well worthwhile.

6 References

Ai, S. et al. (Mar. 2019). "High-precision ice-flow velocities from ground observations on Dalk Glacier, Antarctica". In: *Polar Science* 19, pp. 13–23.

Akhtar, M., N. Ahmad, and M. J. Booij (June 2008). "The impact of climate change on the water resources of Hindukush–Karakorum–Himalaya region under different glacier coverage scenarios". In: *Journal of Hydrology* 355.1-4, pp. 148–163.

Allstadt, K. E. et al. (Dec. 2015). "Observations of seasonal and diurnal glacier velocities at Mount Rainier, Washington, using terrestrial radar interferometry". In: *Cryosphere* 9.6, pp. 2219–2235.

Bauder, A. et al. (2008). "On the outburst of glacier-dammed lakes: Gornergletscher, Valais". In: *Bull. angew. Geol* 13.2, pp. 17–21.

Benoit, L. et al. (Apr. 2019). "A high-resolution image time series of the Gorner Glacier - Swiss Alps - derived from repeated unmanned aerial vehicle surveys". In: *Earth System Science Data* 11.2, pp. 579–588.

Bhardwaj, A. and L. Sam (Aug. 2022). "Editorial: Applications of Remote Sensing in Glaciology". In: *Remote Sensing 2022, Vol. 14, Page 4146* 14.17, p. 4146.

Biondi, F., C. Clemente, and D. Orlando (Sept. 2019). "An atmospheric phase screen estimation strategy based on multichromatic analysis for differential interferometric synthetic aperture radar". In: *IEEE Transactions on Geoscience and Remote Sensing* 57.9, pp. 7269–7280.

Bliss, A., R. Hock, and V. Radić (Apr. 2014). "Global response of glacier runoff to twenty-first century climate change". In: *Journal of Geophysical Research: Earth Surface* 119.4, pp. 717–730.

Bundesamt für Landestopografie swisstopo (2021). *Swiss Map*. Zurich.

Caduff, R., A. Kos, et al. (2014). "Terrestrial radar interferometric measurement of hillslope deformation and atmospheric disturbances in the Illgraben debris-flow catchment, Switzerland". In: *IEEE Geoscience and Remote Sensing Letters* 11.2, pp. 434–438.

Caduff, R., F. Schlunegger, et al. (Feb. 2015). "A review of terrestrial radar interferometry for measuring surface change in the geosciences". In: *Earth Surface Processes and Landforms* 40.2, pp. 208–228.

Caduff, R., T. Strozzi, and A. Wiesmann (2013). "Erfolgreicher Einsatz terrestrischer Radar-Interferometrie zur flächenhaften Vermesung von ausserordentlichen Hangrutschungsbewegungen im Gebiet Hintergraben (OW)". In: *Swiss Bull, angew. Geol* 18.2, pp. 129–138.

Clarke, G. K. (1987). "A short history of scientific investigations on glaciers". In: *Journal of Glaciology* 33.S1, pp. 4–24.

Data availability - MeteoSwiss (n.d.). Accessed: 15.11.2022. URL: `https://www.meteoswiss.admin.ch/weather/measurement-systems/land-based-stations/data-availability.html`.

Ferretti, A. et al. (2007). "InSAR Principles (part A): Guidelines for SAR Interferometry Processing and Interpretation (TM-19, February 2007)". In: *InSAR Principles* February, p. 71.

Fischer and Andrea (2013). "Remote sensing vs. in situ measurements: Two poles of the same planet?" In: *EGUGA* 15, pp. 2013–3220.

Fischer, L. et al. (Sept. 2006). "Geology, glacier retreat and permafrost degradation as controlling factors of slope instabilities in a high-mountain rock wall: the Monte Rosa east face". In: *Natural Hazards and Earth System Sciences* 6.5, pp. 761–772.

Fu, L., J. Guo, and X. Chen (Aug. 2021). "Measurement of ice flow velocities from GPS positions logged by short-period seismographs in East Antarctica". In: *Science China Earth Sciences* 64.8, pp. 1381–1389.

GLIMS Consortium (2005). *GLIMS Glacier Database, Version 1.* Accessed: 20.01.2023. Boulder, Colorado, USA.

Goldstein, R. M. and C. L. Werner (Nov. 1998). "Radar interferogram filtering for geophysical applications". In: *Geophysical Research Letters* 25.21, pp. 4035–4038.

Houghton, J. E. T. et al. (Dec. 2001). "Climate Change 2001: The Scientific Basis". In: *Contribution of Working Group I to the Third Assessment Report of the Intergovernmental Panel on Climate Change (IPCC).* Vol. 881, p. 881.

Hugonnet, R. et al. (Apr. 2021). "Accelerated global glacier mass loss in the early twenty-first century". In: *Nature 2021 592:7856* 592.7856, pp. 726–731.

Huss, M. and R. Hock (Jan. 2018). "Global-scale hydrological response to future glacier mass loss". In: *Nature Climate Change 2018 8:2* 8.2, pp. 135–140.

Huss, M., R. Hock, et al. (Apr. 2012). "Conventional versus reference-surface mass balance". In: *Journal of Glaciology* 58.208, pp. 278–286.

Iannini, L. and A. Monti Guarnieri (May 2011). "Atmospheric phase screen in ground-based radar: Statistics and compensation". In: *IEEE Geoscience and Remote Sensing Letters* 8.3, pp. 537–541.

Iglesias, R. et al. (2014). "Atmospheric phase screen compensation in ground-based sar with a multiple-regression model over mountainous regions". In: *IEEE Transactions on Geoscience and Remote Sensing* 52.5, pp. 2436–2449.

Immerzeel, W. W. et al. (Dec. 2019). "Importance and vulnerability of the world's water towers". In: *Nature 2019 577:7790* 577.7790, pp. 364–369.

Irarrazaval, I. et al. (June 2021). "Determining the evolution of an alpine glacier drainage system by solving inverse problems". In: *Journal of Glaciology* 67.263, pp. 421–434.

Islam, A. et al. (Oct. 2022). "Ceramic membrane for water filtration: Addressing the various concerns at once". In: *Chemical Engineering Journal* 446, p. 137386.

Jouvet, G. et al. (Feb. 2020). "In situ measurements of the ice flow motion at Eqip Sermia Glacier using a remotely controlled unmanned aerial vehicle (UAV)". In: *Geoscientific Instrumentation, Methods and Data Systems* 9.1, pp. 1–10.

Kääb, A., J. M. Reynolds, and W. Haeberli (2005). "Glacier and Permafrost Hazards in High Mountains". In: pp. 225–234.

Kaser, G. et al. (Mar. 2004). "Modern glacier retreat on Kilimanjaro as evidence of climate change: observations and facts". In: *International Journal of Climatology* 24.3, pp. 329–339.

Klingele, E. and H. G. Kahle (July 1977). "Gravity profiling as a technique for determining the thickness of glacier ice". In: *Pure and Applied Geophysics PAGEOPH* 115.4, pp. 989–998.

Kneib-Walter, A., M. P. Lüthi, M. Funk, et al. (Sept. 2022). "Observational constraints on the sensitivity of two calving glaciers to external forcings". In: *Journal of Glaciology*, pp. 1–16.

Kneib-Walter, A., M. P. Lüthi, L. Moreau, et al. (May 2021). "Drivers of recurring seasonal cycle of glacier calving styles and patterns". In: *Frontiers in Earth Science* 9, p. 667717.

Li, X. et al. (June 2016). "Ice flow dynamics and mass loss of Totten Glacier, East Antarctica, from 1989 to 2015". In: *Geophysical Research Letters* 43.12, pp. 6366–6373.

Lillesand, T. M., R. W. Kiefer, and J. W. Chipman (2015). *Remote Sensing and Image Interpretation*. 7th ed. Wiley.

Lüthi, M. P. (Apr. 2014). "Little Ice Age climate reconstruction from ensemble reanalysis of Alpine glacier fluctuations". In: *Cryosphere* 8.2, pp. 639–650.

Lüthi, M. P., A. Bauder, and M. Funk (Dec. 2010). "Volume change reconstruction of Swiss glaciers from length change data". In: *Journal of Geophysical Research: Earth Surface* 115.F4, p. 4022.

Lüthi, M. P. and A. Bauder (June 2010). "Analysis of Alpine glacier length change records with a macroscopic glacier model". In: *Geographica Helvetica* 65.2, pp. 92–102.

Luzi, G. et al. (Nov. 2004). "Ground-based radar interferometry for landslides monitoring: Atmospheric and instrumental decorrelation sources on experimental data". In: *IEEE Transactions on Geoscience and Remote Sensing* 42.11, pp. 2454–2466.

Miteva, V. (2008). "Bacteria in snow and glacier ice". In: *Psychrophiles: From Biodiversity to Biotechnology*, pp. 31–50.

Monserrat, O., M. Crosetto, and G. Luzi (2014). "A review of ground-based SAR interferometry for deformation measurement". In: *ISPRS Journal of Photogrammetry and Remote Sensing* 93, pp. 40–48.

Ouyed Hernandez, A. et al. (Dec. 2020). "Two-Stage Artificial Intelligence Algorithm for Calculating Atmospheric Motion Vectors". In: *AGU Fall Meeting Abstracts*. Vol. 2020, A059-0015, A059–0015.

Palmer, L. (Feb. 2022). "Storing frozen water to adapt to climate change". In: *Nature Climate Change 2022 12:2* 12.2, pp. 115–117.

Pörtner, H.-O. et al. (2019). "The ocean and cryosphere in a changing climate". In: *IPCC special report on the ocean and cryosphere in a changing climate* 1155.

Renaud, A. (1952). "Observations on the Surface Movement and Ablation of the Gorner Glacier (Switzerland)". In: *Journal of Glaciology* 2.11, pp. 54–57.

Ryser, C. et al. (June 2013). "Cold ice in the ablation zone: Its relation to glacier hydrology and ice water content". In: *Journal of Geophysical Research: Earth Surface* 118.2, pp. 693–705.

Sagredo, E. A. and T. V. Lowell (Apr. 2012). "Climatology of Andean glaciers: A framework to understand glacier response to climate change". In: *Global and Planetary Change* 86-87, pp. 101–109.

Strozzi, T., U. Wegmuller, et al. (Nov. 2001). "Land subsidence monitoring with differential SAR interferometry". In: *Photogrammetric Engineering and Remote Sensing* 67.11.

Strozzi, T., C. Werner, et al. (2012). "Topography mapping with a portable real-aperture radar interferometer". In: *IEEE Geoscience and Remote Sensing Letters* 9.2, pp. 277–281.

Sugiyama, S. et al. (Sept. 2010). "Surface ice motion deviating toward the margins during speed-up events at Gornergletscher, Switzerland". In: *Journal of Geophysical Research: Earth Surface* 115.F3, p. 3010.

Vincent, C. (Oct. 2002). "Influence of climate change over the 20th Century on four French glacier mass balances". In: *Journal of Geophysical Research: Atmospheres* 107.D19, pp. 4–1.

Voytenko, D. (Jan. 2015). "Glaciological Applications of Terrestrial Radar Interferometry". In: *USF Tampa Graduate Theses and Dissertations*.

Voytenko, D. et al. (2012). "Monitoring a glacier in southeastern Iceland with the portable Terrestrial Radar Interferometer". In: *International Geoscience and Remote Sensing Symposium (IGARSS)*.

Vuille, M. et al. (Aug. 2008). "Climate change and tropical Andean glaciers: Past, present and future". In: *Earth-Science Reviews* 89.3-4, pp. 79–96.

Wang, Z. et al. (Jan. 2021). "Quantitative analysis of Arctic ice flow acceleration with increasing temperature". In: *Acta Oceanologica Sinica* 40.1, pp. 22–32.

Werner, C. et al. (2009). "A ground-based real-aperture radar instrument for differential interferometry". In: *IEEE National Radar Conference - Proceedings*. ISSN: 10975659.

Zebker, H. A., P. A. Rosen, and S. Hensley (Apr. 1997). "Atmospheric effects in interferometric synthetic aperture radar surface deformation and topographic maps". In: *Journal of Geophysical Research: Solid Earth* 102.B4, pp. 7547–7563.

Zemp, M. et al. (Apr. 2019). "Global glacier mass changes and their contributions to sea-level rise from 1961 to 2016". In: *Nature 2019 568:7752* 568.7752, pp. 382–386.

Zhou, X., N. B. Chang, and S. Li (Mar. 2009). "Applications of SAR interferometry in earth and environmental science research". In: *Sensors* 9.3, pp. 1876–1912.

Appendix A - Python Scripts

Algorithm 1

```
# extact phase information along a line from a series of SLC files
# stored in a hdf5 data set
# this hdf5 data set was created by store_timeseries_hdf5.py from the SLCs

import os
import numpy as np
import scipy.signal
from scipy.signal import detrend
from datetime import datetime

import tables                     # pytables hdf5 library
import scipy.cluster.hierarchy    # curve clustering
import time

env = "tux"

if env == "tux":
    datafile = '/home/anja/work/20221210_142713_allData_mr_hut_2021_slc.h5'
    workpath = '/home/anja/work'
else:
    # on client
    datafile = 'C:/Users/anjas/20230108_191502_600_800_mr_hut_2021_slc.h5'
    workpath = 'C:/Users/anjas/OneDrive/UZH/master_thesis/Code'

os.system('mkdir -p %s' % workpath)

# time limits of good, low-noise data
tlimits = {2021: (0, 1500000.0)}
year = 2021

# algorithm parameters
dp_max   = 4    # max phase jump, above which we unwrap
min_mag  = 0.3  # min signal strength (magnitude)

# some constants
twopi      = 2*np.pi
phase2m    = 0.0087209/twopi      # wavelength / 2 = 0.0087209
ms2md      = 3600 * 24            # conversion from m/s to m/d
dr         = 0.75                 # m; range_pixel_spacing

```

```
41 print('read time')
42
43 h5file = tables.open_file(datafile, mode='r')
44 root   = h5file.root
45
46 # Selection of Data (take every x sample)
47 xtimes = [1, 2, 10, 30]
48
49 # get shape of data
50 # ntime = number of measurements over time
51 # nas = number of range samples on one azimuth line
52 # ras = number of azimuth lines
53 ntime, nas, nrs, _ = root.slc.shape
54
55 # use only subset of azimuth lines
56 azi0 = 100
57 azi1 = 200
58 nas = azi1-azi0
59
60 tsts, _, _ = np.intersect1d(root.time[:], root.time[:], assume_unique=True, return_indices=True)
61
62 # create real time, and time in seconds
63 times = np.array([np.datetime64(datetime.fromtimestamp(t)) for t in tsts])
64 ts    = tsts-tsts[0]     # time difference in seconds
65
66 l = 0
67
68 for x in xtimes:
69
70     start_time = time.time()
71     print(start_time)
72     print('each ' + str(x) + 'time sample')
73
74     # pre-allocate array to collect all velocitites
75     allv_slc   = np.zeros((nas, nrs), dtype=float) + np.nan
76
77     # pre-allocate array for data
78     cdata = np.zeros((ntime, nrs), dtype=complex)
79
80     pPrint1   = []
81     puPrint1  = []
82     pndPrint1 = []
83     dpPrint1  = []
84
85     pPrint2   = []
```

```
86      puPrint2  = []
87      pndPrint2 = []
88      dpPrint2  = []
89
90      azino1 = None
91      azino2 = None
92      rngno1 = None
93      rngno2 = None
94
95      aziLine = []
96      aziLineC =  []
97
98
99      # loop over the azimuth lines
100     for azi, c in zip(range(azi0,azi1)[:], range(nas)[:]):
101         print('processing line', azi)
102
103         print('read data')
104         # reading data from file and represent as complex number
105         cdata[:] = root.slc[:, azi, :, 0].astype(float) + 1j*root.slc[:, azi, :, 1].astype(float)
106
107         print('calc phase')
108
109         # limit to useful time span
110         t0, t1 = tlimits[year]
111         tidx = (t0 <= ts) & (ts <= ts)
112
113         tt = ts[tidx]
114         tt = tt[0::x]
115
116         phase = np.angle(cdata[:])
117         phase = phase[0::x]
118
119         # mag   = np.abs(cdata[0::x].mean(1))
120         mag   = np.abs(cdata[:].mean(1))
121         mag = mag[0::x]
122
123         # mean signal magnitude per range sample
124         magmean = np.abs(cdata[:]).mean(0)
125
126         # range indizes for good enough signal
127         rid = np.nonzero(magmean > min_mag)[0]
128
129         # loop over the pixels of this line and figure out time changes of phase
130         allm   = []
```

```
131         allpnd = []
132         allmpm = []
133 
134         # loop over the range samples of this azimuth line
135         for i in range(0, nrs):
136             # skip pixels with no good  data
137             if magmean[i] < min_mag:
138                 continue
139 
140             # get phase of one range sample over time
141             p  = phase[:, i]
142 
143             # find phase noise
144             # phase unwrapping
145             pu = np.unwrap(p, dp_max)
146 
147             # detrend the phase to get the noise
148             pnd = detrend(pu)
149 
150             allpnd.append(pnd)
151 
152             if azi==100 and i==600:
153                 azino1 = azi
154                 rngno1 = i
155 
156                 pPrint1 = p
157                 puPrint1 = pu
158                 pndPrint1 = pnd
159 
160                 aziLine = phase
161             elif azi==195 and i==870:
162                 azino2 = azi
163                 rngno2 = i
164 
165                 pPrint2 = p
166                 puPrint2 = pu
167                 pndPrint2 = p
168 
169         allpnd = np.array(allpnd)
170 
171         # cluster the phase noise curves to determine the mean phase noise
172         Z      = scipy.cluster.hierarchy.linkage(allpnd, method='average')
173         idxs   = scipy.cluster.hierarchy.fcluster(Z, 8, criterion='maxclust')
174 
175         # find the mean phase noise deviation of the maximum cluster
```

```
176         maxidx = np.bincount(idxs).argmax()
177         pnd_mean = allpnd[idxs == maxidx].mean(0)
178 
179         # now subtract the mean phase noise from all points on the line,
180         # then unwrap, and determine the rate of phase change (=> velocity)
181 
182         print('process line')
183         allpv = []
184         for i in range(0, nrs):
185             if (not i in rid):
186                 continue
187             if magmean[i] < min_mag:
188                 continue
189             p = phase[:,i]
190             dp = p - pnd_mean
191 
192             if azi==azino1 and i==rngno1:
193                 dpPrint1 = dp
194                 aziLineC = pnd_mean
195             elif azi==azino2 and i==rngno2:
196                 dpPrint2 = dp
197 
198             dpu = np.unwrap(dp, dp_max)
199 
200             # run polyfit to get the slope of the trend
201             param = np.polyfit(tt, dpu, 1)
202             allv_slc[c, i] = param[0]
203 
204     allv_slc *= (phase2m * ms2md)
205 
206     dt = datetime.now()
207     timestamp = dt.strftime("%Y%m%d") + '_' + dt.strftime("%H%M%S")
208     whatitis = '_600_800_'
209 
210     np.save('results/' + timestamp + whatitis + '_slc_' + str(x) + '.npy', allv_slc)
211     with open('results/' + timestamp + whatitis + '_exeTime_slc_' + str(x) +'.txt', 'w') as f:
212         f.write(str((time.time() - start_time)))
```

Appendix B - Personal Declaration

I hereby declare that the material contained in this thesis is my own original work. Any quotation or paraphrase in this thesis from the published or unpublished work of another individual or institution has been duly acknowledged. I have not submitted this thesis, or any part of it, prieviously to any institution for assessment purposes.

Zurich, 31.01.2023
Place, Date

Signature